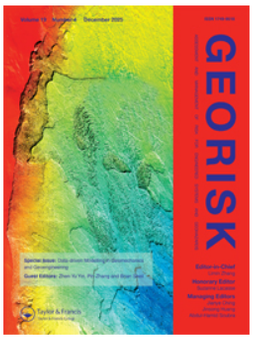

Georisk: Assessment and Management of Risk for Engineered Systems and Geohazards

ISSN: 1749-9518 (Print) 1749-9526 (Online) Journal homepage: www.tandfonline.com/journals/ngrk20

Optimal ground motion intensity measures for the seismic vulnerability assessment of embankment dams

Surya Prakash & P. Anbazhagan

To cite this article: Surya Prakash & P. Anbazhagan (18 Jan 2026): Optimal ground motion intensity measures for the seismic vulnerability assessment of embankment dams, Georisk: Assessment and Management of Risk for Engineered Systems and Geohazards, DOI: 10.1080/17499518.2026.2614741

To link to this article: https://doi.org/10.1080/17499518.2026.2614741

Published online: 18 Jan 2026.

GEORISK
https://doi.org/10.1080/17499518.2026.2614741

Taylor & Francis
Taylor & Francis Group

Optimal ground motion intensity measures for the seismic vulnerability assessment of embankment dams

Surya Prakash and P. Anbazhagan

Department of Civil Engineering, Indian Institute of Science, Bangalore, India

ABSTRACT

The seismic response of embankment dams is critical for effective seismic design, yet probabilistic seismic demand models (PSDMs) for these structures remain underexplored. This study develops PSDMs to identify the optimal Intensity Measure (IM) for embankment dams by evaluating 14 different IMs. Two approaches are employed for PSDM development: one utilises empirical data from earthquake records from instrumented embankment dams, while the other is based on numerical simulations using a Finite Element Method model of dam subjected to ground motion records from free-field and dam site stations. A novel fuzzy comprehensive IM evaluation framework is proposed, and using this framework, it was found that Root Mean Square Velocity (VRMS) from empirical PSDM and Peak Ground Velocity (PGV) from the numerical analysis PSDM are the most optimal IMs. In contrast, Effective Design Acceleration is least optimal IM across both approaches. The study then classifies dam damage into five states using relative crest settlement ratio as the engineering demand parameter. Seismic fragility analysis conducted through both PSDM approaches indicates that Peak Ground Acceleration, a commonly used IM, significantly underestimates the probability of damage to embankment dams, with maximum underestimations of 44% and 30% observed using the empirical and numerical PSDMs, respectively.

ARTICLE HISTORY
Received 4 June 2025
Accepted 2 January 2026

KEYWORDS
Seismic vulnerability; embankment dams; fuzzy evaluation method; optimal intensity measure; fragility curves

1. Introduction

Embankment dams are essential for water conservation, domestic water supply, agricultural irrigation, and industrial use (Beck, Claassen, and Hundt 2012; Busch 2021). Additionally, these structures produce hydroelectric power, which lessens reliance on fossil fuels and provides renewable energy (Schleiss 2018). Furthermore, by reducing storm surges and heavy rainfall, these dams are essential for flood control (Chen et al. 2021). Their design and construction must carefully consider environmental challenges like water level changes and flooding risks (Adamo et al. 2020; Zheng et al. 2023). A major safety risk is their susceptibility to seismic activity, as earthquakes can threaten their stability, potentially causing catastrophic flooding, loss of life, and significant environmental and financial damage (Gordan et al. 2021; Liu et al. 2015; L. M. Zhang, Xu, and Jia 2009).

The seismic safety evaluation of embankment dams has evolved significantly over the past decades, progressing from simplified deterministic analyses to advanced numerical and probabilistic frameworks. Early assessment methods were largely empirical and relied on expert judgment or damage observations from past earthquakes (Xu and Pang 2024). However, limited case data and high site-specific variability make their use less frequent. Pseudo-static analysis, one of the first systematic approaches, applies an equivalent horizontal seismic coefficient but oversimplifies transient effects, resulting in conservative safety factors (Akhlaghi and Nikkar 2014; Seed 1965). The Newmark sliding-block model (Newmark 1965) enhanced this framework by estimating cumulative displacements once ground accelerations exceed a threshold yield acceleration, and it has been widely used for crest settlement estimation (Regina et al. 2023). Nevertheless, assumptions of rigid-block behaviour neglect distributed deformations, cracking, and pore-pressure effects.

Advances in computational tools have established the numerical modelling methods like finite-element method (FEM) and finite-difference method (FDM) as standards for seismic evaluation of dams (Regina et al. 2023; Xu and Pang 2024). These models capture dam–foundation–reservoir interaction, nonlinear material behaviour, pore-pressure buildup, and complex geometries. Experimental methods, such as shaking-table and centrifuge tests, field monitoring with piezometers and weirs, and geotechnical investigations of liquefaction

CONTACT P. Anbazhagan anbazhagan@iisc.ac.in Department of Civil Engineering, Indian Institute of Science, Bangalore, Karnataka, India

potential, complement numerical analyses, providing comprehensive seismic safety assessments of embankment dams (Xu and Pang 2024).

Probabilistic methods explicitly quantify uncertainties in ground motion, material properties, and structural behaviour, yielding risk-based rather than deterministic outcomes. Recent studies have demonstrated the importance of such probabilistic frameworks in dam and geotechnical risk assessment, particularly when integrating monitoring data or characterising geological and hazard-related uncertainties (Jiang et al. 2025; Peng et al. 2024; Qi et al. 2024). Performance-based earthquake engineering (PBEE) represents a widely adopted probabilistic framework that integrates seismic hazard, structural response, and damage or loss estimation to support risk-informed decisions (Huang et al. 2009; Moehle and Deierlein 2004). Originally developed for buildings and bridges, PBEE has been extended to dam safety, where it links intensity measures (IMs) to engineering demand parameters (EDPs) through IM–EDP relationships and fragility curves (Giusto 2025; Tartaglia, D'Aniello, and Landolfo 2022). Enhancing PBEE for dams requires accounting for both human and economic consequences of earthquake-induced damage (Zerbe and Falit-Baiamonte 2001). The framework generally involves site-specific hazard analysis, dam response evaluation, estimation of damage probabilities, and assessment of repair or loss consequences (Heresi and Miranda 2023).

Probabilistic Seismic Demand Models (PSDMs) statistically relate IMs to EDPs, forming the basis for fragility analysis and enabling probabilistic estimation of damage exceedance. Empirical PSDMs use earthquake case histories (Ghaemi and Konrad 2023; Vahedifard and Meehan 2011), while simulation-based PSDMs rely on numerical models calibrated with site data (Macedo 2015). Recent developments in hybrid and machine-learning-based PSDMs have enhanced computational efficiency and predictive capability (Mohammad Amin Hariri-Ardebili, Chen, and Mahdavi 2022; Salazar and Hariri-Ardebili 2022) but remain exploratory. Existing PSDMs are often developed for specific types of dams. To the author's knowledge, PSDMs directly derived from instrumented dam's data have not been systematically developed, and no study has built PSDMs and fragility curves in parallel using both empirical and numerical data-based PSDMs for embankment dams. Comparable efforts have been made for levees; Kwak et al. (2016) characterised the seismic fragility of levees using field performance data, and Liu (2024) conducted a system-level seismic risk assessment of California's levees, highlighting the potential for integrated studies in embankment dams.

Within the PBEE framework, selecting an appropriate IM is a crucial step, as the dispersion of EDPs and the uncertainty of fragility functions are highly dependent on the chosen IM (Huang et al. 2021). Traditional PSDMs commonly rely on a single IM, generally Peak Ground Acceleration (PGA). Recent studies have explored alternative IMs that better represent ground motion complexity and its influence on dam response (Armstrong, Kishida, and Park 2020; Khalid et al. 2023; Regina et al. 2023). Arias Intensity (AI) has been identified as a reliable predictor of deformation in earth dams (Armstrong, Kishida, and Park 2020). Similarly, Khalid et al. (2023) demonstrated that Effective Design Acceleration (EDA), Sustained Maximum Acceleration (SMA), Root Mean Square Acceleration (ARMS), Peak Ground Velocity (PGV), and Characteristic Intensity (IC) provide improved predictive performance for concrete-faced rockfill dams. Regina et al. (2023) further demonstrated that Cumulative Absolute Velocity (CAV) is particularly effective in capturing the nonlinear deformation behaviour of earthen dams through FEM analyses. Hence, the optimal choice of IM varies across different dam types, and most of the existing IM evaluations are commonly based on simulation-based PSDM. To the author's knowledge, instrumented embankment dam seismic record data have not yet been systematically used for either PSDM development or IM evaluation, and no study has systematically evaluated candidate IMs using both empirical and simulation data within a unified framework, underscoring the need for integrated research to reduce uncertainty in PSDM predictions for embankment dams.

The present study evaluates a range of candidate IMs that are critical for assessing the seismic vulnerability of embankment dams. Fourteen IMs influencing dam response are considered and grouped into frequency, energy, and amplitude based IMs. Probabilistic Seismic Demand Models (PSDMs) are developed using two complementary approaches: the first employs empirical data from earthquake records from instrumented embankment dams, while the second relies on FEM simulations of a homogeneous embankment dam subjected to recorded ground motions. The empirical PSDM yields IMs that are broadly applicable to different types of embankment dams, whereas the numerical PSDM provides optimal IMs applicable to homogeneous embankment dams. The performance of each IM is assessed in terms of efficiency, practicality, and proficiency. A structured fuzzy logic evaluation framework is proposed to integrate these criteria and identify the optimal IMs for assessing the seismic vulnerability

of embankment dams. Finally, seismic fragility analyses are conducted using both empirical and numerical PSDMs to ensure a consistent and reliable evaluation of dam performance.

The novelty of this work includes developing empirical and numerical data-based PSDM within a unified framework to enhance the reliability of optimal IM selection and vulnerability assessment of embankment dams. The research advances existing studies by introducing a structured fuzzy logic–based evaluation framework and, for the first time, proposing optimal IM applicable to different types of instrumented embankment dams and homogeneous embankment dams. Furthermore, the study establishes seismic fragility curves derived from both empirical and simulation-based PSDMs, providing a comprehensive and consistent basis for the seismic vulnerability assessment of embankment dams.

2. Ground motion intensity measures

Amplitude, frequency content, and duration are among the attributes of ground motion intensity measures (IMs) that are essential for evaluating the performance and safety of structures (Kramer and Stewart 2024; Zhang et al. 2025). Selecting appropriate IMs is crucial when developing IM-EDP relations for embankment dams to accurately gauge seismic vulnerability. Common IMs include peak ground acceleration (PGA), peak ground velocity (PGV), and spectral acceleration (Sa) at various periods. With the increasing availability of recorded ground motion data, modern IMs have been developed to capture additional aspects of seismic excitation and improve correlations with EDPs. In this study, fourteen representative IMs were derived from earthquake acceleration time histories using SeismoSignal software (Seismosoft 2024). These IMs encompass the three principal families widely recognised in earthquake engineering: amplitude-based (PGA, PGV, PGD, SMA, SMV, EDA), frequency-based (ARMS, VRMS, DRMS, PGV/PGA, PP, MP), and energy-based (AI, CAV). Together, these measures capture the primary factors that control the response of geotechnical systems (Housner 1952; Arias 1970; USACE 2024). The selected IMs are consistent with standard engineering practice and follow FEMA and USACE guidelines, which recommend PGA, PGV, PGD, and spectrum-based measures for assessing the effects of ground motion on critical infrastructure (FEMA 2020; USACE 2007).

Some less-commonly used IMs, such as particular definitions of significant duration and cumulative squared acceleration (CSA), were not included in this study. This choice preserves interpretability by limiting IMs that convey very similar information. Duration-related and cumulative effects are already represented by AI, CAV, ARMS, and VRMS, while spectral and period-based measures capture frequency content and resonance potential. CSA is proportional to the time integral of acceleration squared and is therefore closely related to AI. Studies have shown that AI and CSA are strongly correlated and that CSA adds little extra predictive value for most geotechnical applications (Arias 1970; Baltay, Hanks, and Abrahamson 2019; Bradley 2015). Table 1 summarises these IMs and their typical use in dam and soil structure, while detailed definitions are provided in Appendix A.

3. IM-EDP relationship

Evaluating structural performance under dynamic loads requires an understanding of the relationship between IMs and EDPs. IMs show the severity of ground motion, whereas EDPs show structural responses (Rathje and He 2022). Evaluations of seismic risk are improved by a strong IM-EDP correlation. Pinzón et al. (2023) demonstrate that metrics like Sa at a building's fundamental period correlate with EDPs more closely than more traditional IMs like PGA, supporting the idea that structural dynamics should be added to IMs. To predict seismic-induced deformations and maintain structural integrity, IM-EDP relationships are essential for embankment dams. The choice of IM has a major impact on crest settlements and failure probabilities, so specific IM-EDP relation models are required for seismic evaluations (Rathje and He 2022). Accurate estimates of earthquake-induced displacements require detailed analyses, as probabilistic seismic hazard analyses (PSHA) often miss complex structural responses (Ghahreman-Nejad and Kan 2017). Thus, specialised analyses within the PBEE framework are vital for assessing the seismic performance of embankment dams.

PSDMs are utilised to describe the seismic response of structures by defining a probabilistic relation between ground motion IMs and EDPs (Regina et al. 2023). These models are founded on the assumptions that EDPs are distributed lognormally; there exists a logarithmic, linear relationship between EDP and IM, and the logarithmic standard deviation of EDPs is constant (Cornell et al. 2002). The relationship between EDPs and IMs is expressed through a power function, as outlined in Equation (1):

$$EDP = a\,(IM)^b \tag{1}$$

where, a and b are regression coefficients derived from regression analysis, while EDP is the engineering

Table 1. Intensity measures considered in the current study, with their physical meaning and application in the context of the dam and soil structure.

Category	Intensity measure (IM)	Notation	Physical meaning	Application (dam/soil structure)
Amplitude Based	Peak Ground Acceleration(*g*)	PGA[1]	Maximum ground acceleration	Common seismic hazard parameter; primary input for pseudo-static stability checks and force-based analysis (Papadimitriou, Bouckovalas, and Andrianopoulos 2014).
	Peak Ground Velocity(*m/s*)	PGV[1]	Maximum ground velocity	Strongly correlates with liquefaction triggering and velocity-dependent embankment deformations and displacements (USACE 2024).
	Peak Ground Displacement(*m*)	PGD[1]	Maximum ground displacement	Assesses long-period demands. Indicates residual settlement and permanent slope movement (Kramer and Stewart 2024).
	Sustained Maximum Acceleration(*g*)	SMA[2]	Third-largest cyclic acceleration peak	Highlights prolonged cyclic accelerations affecting the crest. Represents sustained shaking that increases cyclic degradation (Yakut and Yılmaz 2008).
	Sustained Maximum Velocity(*m/s*)	SMV[2]	Third-largest cyclic velocity peak	Evaluates velocity-sensitive deformation. Captures velocity pulses driving cumulative displacement (Yakut and Yılmaz 2008).
	Root-mean-square of Acceleration(*g*)	ARMS[4]	Root-mean-square acceleration	Represents average shaking intensity; used in random vibration theory for demand estimation.
	Root-mean-square of Velocity (*m/s*)	VRMS[4]	Root-mean-square velocity	Assesses long-period energy for embankment response. Supports displacement/liquefaction correlations.
	Root-mean-square of Displacement(*m*)	DRMS[4]	Root-mean-square displacement	Indicates low-frequency and long-wave energy content; relevant for large structures.
	Effective Design Acceleration(*g*)	EDA[6]	PGA filtered above ~*8–9 Hz*	Filters irrelevant high-frequency content for demand estimation. Prevents overestimation from instrument noise (Kennedy et al. 1980).
Frequency Based	The ratio of PGV to PGA (*s*)	PGV| PGA[1]	Proxy for characteristic period (≈*T/2π*)	Distinguishes between short-period and long-period motions and is a key spectral shape parameter (Rathje, Abrahamson, and Bray 1998).
	Predominant Period (*s*)	PP[1]	Period of maximum spectral acceleration	Identifies dominant motion frequency; critical for resonance studies with the structure's natural period.
	Mean Period (*s*)	MP[3]	Fourier amplitude-weighted mean period	Simplified descriptor of spectral shape and can be used for site classification (Rathje, Abrahamson, and Bray 1998).
Energy Based	Arias Intensity(*m/s*)	AI[5]	Cumulative squared acceleration content	Measures shaking "energy"; highly effective in predicting cracking, slope sliding, and liquefaction potential in earth structures (Reed and Kassawara 1990).
	Cumulative Absolute Velocity(*m/s*)	CAV[1]	Time integral of absolute acceleration	Used as a cumulative damage index in dam safety assessments for distinguishing damaging vs. non-damaging motions (Reed and Kassawara 1990).

[1]Kramer and Stewart (2024); [2]Nuttli (1979); [3]Rathje, Abrahamson, and Bray (1998); [4]Housner and Jennings (1964); [5]Arias (1970); [6]Benjamin (1988).

demand parameter. The assumption of a power function relationship, as described above, has been widely applied in the fragility analysis of various structural systems. Additionally, Equation (1) can be reformulated into the form of a logarithmic normal linear regression model, provided that the seismic demand follows a log-normal distribution (Dhiman et al. 2024; Lee et al. 2019), as illustrated in Equation (2):

$$\ln(EDP) = ln(a) + b \cdot \ln(IM) \quad (2)$$

where a and b represent the antilogarithm and slope of the perpendicular offset in the PSDM relationship. The following two primary methodologies can establish the relationship between the IM and the EDP using PSDM:

3.1. Method 1: empirical analysis (using earthquake records from instrumented dams)

An empirical PSDM is constructed using observed data rather than numerical simulations. This data can come from post-earthquake damage surveys that analyze how structures performed during past earthquakes (Khanmohammadi et al. 2023; Lozano and Tien 2023; Lulić et al. 2021), experimental testing through shake table experiments to observe structural responses (Cui 2023; Hu et al. 2021), and instrumented structures (e.g. buildings and dams) collecting real-time data from structures equipped with sensors during seismic events (Adamo et al. 2020; Clarkson, Williams, and Seppälä 2020; S. Wang et al. 2024).

Empirical studies have demonstrated a strong correlation between accumulated vertical displacement, particularly the maximum observed vertical displacement at a dam's crest following seismic events, and IM metrics such as PGA and Sa. For example, Nardo, Biondi, and Cascone (2024) investigated the San Pietro Dam and identified relationships between crest vertical displacements and seismic parameters, ultimately developing empirical equations for predicting crest settlement. Similarly, De La Paz-Bonilla and Vidot-Vega (2017) concentrated on crest settlements at the Carite Dam, relating them to Sa.

We developed the empirical PSDM using earthquake records from instrumented embankment dams. Acceleration records from instrumented dam crests were processed using SeismoSignal (Seismosoft 2024) through a two-stage digital signal processing workflow as discussed by Boore and Bommer (2004). From the displacement time histories produced, peak and cumulative vertical crest displacements were extracted for

performance-based seismic assessment (Han et al. 2019; Priestley and Kowalsky 2000). The seismic performance of the embankment dam was assessed using the relative crest settlement ratio (RS) as the EDP. Few studies have shown a significant correlation between the damage state of an earth dam and the RS (Fell et al. 2005; Swaisgood 2003). RS is defined as the ratio of the settlement of the dam crest to its total height, expressed as a percentage (He and Rathje 2024):

$$RS\ (\%) = \frac{Crest\ Settlement}{Height\ of\ Dam} \times 100 \tag{3}$$

where the dam crest settlement is the displacement of the dam crest in the vertical direction, and the dam height is the original height of the dam before any deformation. For this method, the crest settlement is taken as the accumulated vertical displacement. A total of 11 instrumented embankment dams were affected by 20 earthquake events, sourced from literature and the COSMOS Strong Motion Data Centre, which were considered for this method and listed in Table 2. Only records with acceleration time histories from the dam toe/downstream/base and crest were selected. In the following texts, this method will be termed as M_1.

3.2. Method 2: numerical simulations (FEM modelling of dam)

For this method, we utilised a sample embankment dam described by Guo, Dias, and Pan (2019), as illustrated in Figure 1(a). This dam has a height of 16 metres, with both the upstream and downstream slopes designed at a ratio of 1:2.6. Table 3 summarises the characteristics of the dam body and foundation materials, as detailed by Guo, Dias, and Pan (2019). These properties include unit weight, effective cohesion, effective friction angle, young's modulus, and poisson's ratio.

A 2D FEM model of the embankment dam was created using the QUAKE W module of GeoStudio software (GEO-SLOPE International Ltd. 2024). Dynamic analyses utilised QUAKE W's nonlinear capabilities under 2D plain-strain conditions. The model consists of two main elements: the dam body and foundational bedrock, as shown in Figure 1(b). The FEM model was developed based on material properties listed in Table 3, with additional assumptions. To ensure a balance between accuracy and computational efficiency, the mesh size was selected to not exceed 1/10 to 1/8 of the wavelength for the highest excitation frequency (Lysmer and Kuhlemeyer 1969); resulting in mesh sizes ranging from 0.5 m to 2 m, we have used a mesh size of 2 m as shown in Figure 1(b). The dam and its foundation do not vibrate independently under external excitation; instead, they behave as a coupled system (Burman et al. 2011). Therefore, the interaction between the dam and the foundation was considered by modelling the embankment and foundation together as deformable continua within the QUAKE W nonlinear dynamic framework (GEO-SLOPE International Ltd. 2024). These zones were meshed as a bonded continuum so that stress transfer and deformation compatibility across the dam–foundation interface were captured directly by the FEM formulation (Chakraborty and Dey 2024; Guo, Dias, and Pan 2019; He and Rathje 2024; Khalilzad, Gabr, and Hynes 2015).

Each simulation was conducted in two distinct phases. In the initial static phase, the boundary constrains the horizontal displacements of the foundation's side face and horizontal and vertical movements at the base. The FEM dam model was then geostatically balanced before dynamic loading. Gravity loading was applied and iterated to equilibrium, and the resulting in-situ stress and pore-water pressure fields were then used to initialise the subsequent nonlinear dynamic analysis, ensuring geostatic stress balance and eliminating any spurious initial displacements before dynamic loading. Residual nodal displacements and unbalanced forces were checked and found to be negligible, allowing for a start to the dynamic analysis from a physically equilibrated state. In the subsequent dynamic phase, the vertical displacements of the foundation's side face and horizontal and vertical movements at the base are restricted, and the coupled response of the dam and foundation under seismic loading is computed. This procedure follows the recommendations of the QUAKE W guidelines (GEO-SLOPE International Ltd 2024) and aligns with recent applications of GeoStudio in seismic slope and dam stability analyses (Chakraborty and Dey 2024; Hongqiang et al. 2025).

Using a linear elastic model could result in calculated stresses in some places that are higher than the strength of the soil, which is not realistic considering the characteristics of the soil, especially during intense seismic activity. For the soil to accurately assess the stress and deformation characteristics, a nonlinear constitutive model must be implemented, guaranteeing that the computed stresses stay within the limits of the soil's strength. To effectively capture the nonlinear response of the dam during seismic events, this study utilised dynamic effective stress analysis. The hyperbolic backbone curve, which adheres to the Masing rule (Kramer and Stewart 2024), was employed to represent the nonlinear stress–strain relationships of the dam materials (Hu et al. 2023). This curve is defined by two key

Table 2. Summary of crest displacement and earthquakes recorded on the dam used in method 1 (M_1).

Dam	H_D (*m*)	Earthquake	Date	Epicentre		Fault Type	Tectonic Setting	D_f (*km*)	M_w	R_{hyp} (*km*)	S (*cm*)	PGA (*g*)
				Lat (°)	Long (°)							
Anderson	72	Alum rock	2017/10 /10	37.43	−122	Right lateral strike-slip	Interplate	9.2	4.1	16.8	0.006	0.004
		Loma Prieta	1989/10/18	37.04	−122	Oblique slip reverse	Interplate	18	6.9	27	159	0.135
		Morgan Hills	1984/04/24	37.31	−122	Right lateral strike-slip	Interplate	8	6.2	4.8	40.70	0.423
Carbon Canyon	30	Northridge	1994/01/17	34.21	−119	Blind thrust	Intraplate	17.5	6.7	67	54.16	0.195
		Whittier Narrows	1987/10/1	34.05	−118	Thrust	Intraplate	14.6	5.9	24.7	23.67	0.319
Cayote	50	Redwood Valley	2017/10/13	39.2	−123.2	Right lateral strike-slip	Interplate	4	4.2	10.8	0.128	0.037
Del Velle	70	Loma Prieta	1989/10/18	37.04	−122	Oblique slip reverse	Interplate	18	6.9	66	248.6	0.055
Long Valley	38.4	Chalfant Valley	1986/07/21	37.58	−118	Right lateral strike-slip	Interplate	19	6.4	26.7	8.256	0.096
		Toms Place	2020/02/1	37.53	−119	Oblique-slip (transtensional)	Interplate	10	4.4	–	0.032	0.05
Martis Creek	34.4	Mohawk valley	2001/08/10	39.8	−120	Right lateral strike-slip	Interplate	14	5.4	72	0.013	0.023
Pacoima	113	Chino hills	2008/07/29	33.96	−118	Oblique slip	Interplate	14.6	5.4	–	0.006	0.006
		Newhall	2011/08/01	34.37	−119	Reverse	Intraplate	7.2	4.2	–	0.001	0.005
San Antonio	49	Lake Nacimiento	2009/06/20	39	−123	Oblique-slip thrust	Intraplate	6.1	4.6	–	0.004	0.023
		Newidria	2012/09/20	36.4	−120.7	Blind thrust	Interplate	9.4	5.3		0.043	0.03
		Parkfield	2005/06/16	35.9	−120	Right lateral strike-slip	Interplate	8.9	3.4	–	0.004	0.028
		San Simeon	2003/12/22	35.71	−121	Blind thrust	Interplate	7.1	6.5	–	1.378	0.116
Tolt River	61	Duval	1996/05/03	47.77	−122	Strike-slip	Intraplate	7	5.1	14.8	1.663	0.183
		Nisqually	2001/02/28	47.18	−122.9	Normal	Intraplate	52	6.8	111	1.092	0.133
Terminus	78	Ridgecrest	2019/07/06	35.76	−118	Strike-slip	Interplate	7	7.1	–	1.049	0.016
Prado	49	Northridge	1994/01/17	34.2	−119	Blind thrust	Intraplate	17.5	6.7	85.4	191	0.193

Abbreviations: Lat: Latitude, long: Longitude, H_D: Height of dam, M_w: Moment magnitude, R_{hyp}: Hypocentral Distance, D_f: Fault Depth, S: Accumulated vertical displacement, PGA: Peak Ground Acceleration.

parameters: the slope at zero strain, known as the initial small-strain shear modulus (G_{max}), and the asymptotes at large strains (shear strength).

The soil properties within the hyperbolic model are relatively straightforward, requiring values for G_{max} along with the Mohr-Coulomb strength parameters (cohesion, c, and angle of internal friction, φ). The initial G_{max} is determined based on effective overburden stress in QUAKE W. In this effective stress nonlinear model, the damping characteristics of the dam parameters are linked to G_{max}, as discussed by Ishibashi and Zhang (1993) as given in Equation (4).

$$D = D_{max}\left(1 - \frac{G}{G_{max}}\right) \tag{4}$$

D_{max} is a user-defined value of maximum damping set in this study at 0.35, while G_{max} denotes the initial small-strain shear modulus. This modulus is derived from the chosen material property function and the initial static effective overburden stress. At the outset of the analysis, G is initialised to G_{max}, and D is the

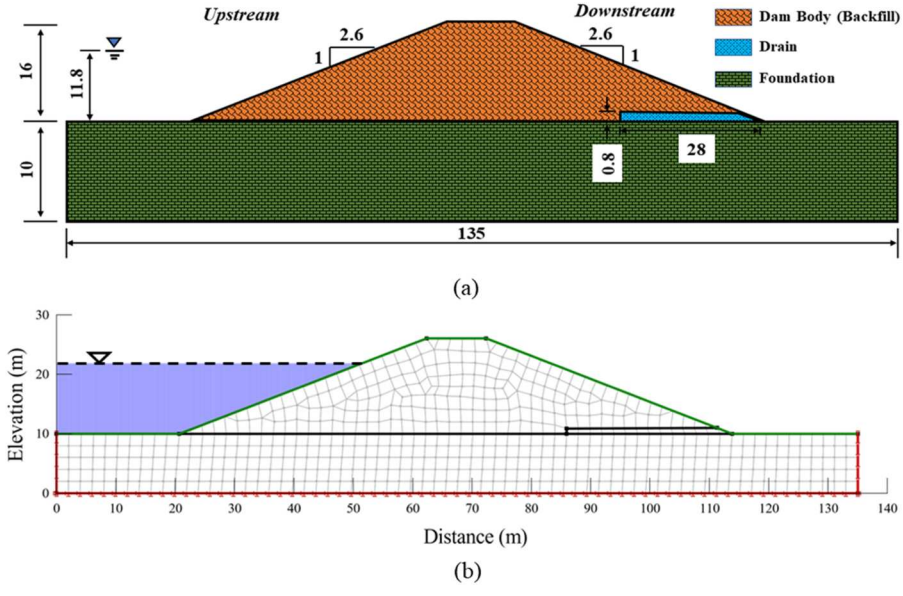

Figure 1. Geometry for finite element modelling of the embankment dam: (a) Embankment dam geometry with different materials represented by distinct colours (adapted from Guo, Dias, and Pan 2019); (b) Schematic view of the model geometry and the corresponding finite element mesh employed in the present study.

Table 3. Soil parameters for the studied embankment dam (After Guo, Dias, and Pan 2019).

Parameters	Dam body (backfill)	Foundation
Effective cohesion (*kPa*)	8.9	100
Effective friction angle (°)	34.8	34.1
Unit weight (kN/m^3)	20	18
Young modulus (*MPa*)	100	600
Poisson's ratio (μ)	0.3	0.25

damping assigned a minimum value of 0.05 for this study. During the dynamic phase, the shear modulus, referred to as G, is modelled according to the shear modulus degradation function developed by Ishibashi and Zhang (1993) in QUAKE W.

A comprehensive series of nonlinear dynamic analyses was performed. Acceleration records from various earthquakes were collected from multiple stations; however, due to a lack of detailed information regarding the seismic hazard analysis of the dam site, the input motion for the model was derived from an earthquake database, specifically selecting records with a PGA $\geq$ 0.05 g. The magnitudes of the earthquakes chosen varied from moment magnitude (M_w) of 5.1 to 7.6, ensuring the inclusion of a range of fault mechanisms and tectonic settings to address all potential types of earthquake sources. Horizontal ground motions were applied at the base of the model, utilising a total of thirty free-field earthquake records from seven distinct earthquakes, along with nine records from eight stations situated on the embankment dam sites. A summary of the input motions used is presented in Table 4, and Figure 2 presents the response spectrum of all input ground motions. Throughout the analyses, vertical displacement was calculated, with results documented for key nodes located at the dam's crest. The seismic response was evaluated based on the maximum vertical displacement recorded at the crest. Figure 3 illustrates an example of the vertical

Table 4. Earthquake records used in Method 2 (M_2) for FEM modelling.

Station location	Earthquake	Date	Fault type	Tectonic setting	D_f (*km*)	M_w	No of records
Free Field	Chichi	1999/09/20	Thrust	Interplate	8	7.7	15
	Kobe	1995/01/16	Right lateral strike-slip	Intraplate	17.6	7.3	7
	Imperial Valley	1979/10/15	Right lateral strike-slip	Interplate	10	6.4	1
	Kozani-Grevena	1995/05/15	Normal	Intraplate	14	6.6	2
	Loma Prieta	1989/10/17	Oblique slip reverse	Interplate	18	6.9	2
	Manjil-Rudbar	1990/06/20	Left lateral strike slip	Intraplate	15	7.4	1
	Westmorland	1981/04/26	Strike-slip	Interplate	10	5.9	2
Anderson Dam	Morgan Hills	1984/04/24	Right lateral strike-slip	Interplate	8	6.2	1
	Loma Prieta	1989/10/18	Oblique slip reverse	Interplate	18	6.9	1
Carbon Canyon Dam	Whittier Narrows	1987/10/1	Thrust	Intraplate	14.6	5.9	1
Long Valley Dam	Chalfant Valley	1986/07/21	Right lateral strike-slip	Interplate	19	6.4	1
Parado Dam	Northridge	1994/01/17	Blind thrust fault	Intraplate	17..5	6.7	1
Seven Oaks Dam	SanBrendo	2009/01/08	Right lateral strike-slip	Interplate	13.8	4.5	1
San Antonio Dam	San Simeon	2003/12/22	Blind Thrust fault	Interplate	7.1	6.5	1
Sant Felica Dam	Northridge	1994/01/17	Blind thrust fault	Intraplate	17.5	6.7	1
Tolt River Dam	Duval	1996/05/03	Strike-slip faulting	Intraplate	7	5.1	1

Abbreviations: M_w: Moment Magnitude, D_f: Fault Depth.

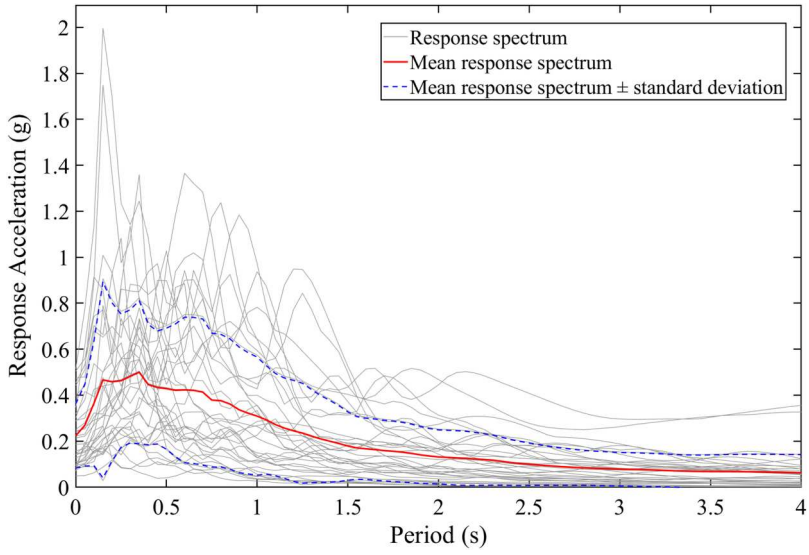

Figure 2. Response acceleration of all considered input ground motions, where the red line denotes the mean response acceleration.

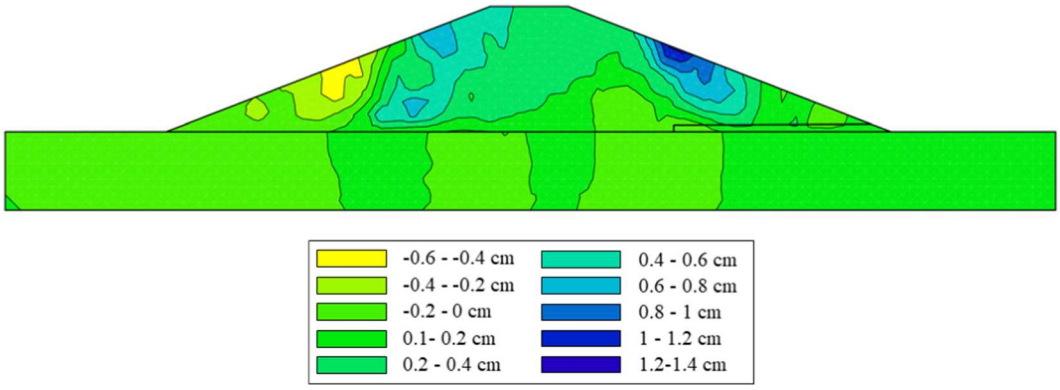

Figure 3. Example of a vertical displacement contour obtained from finite element (FEM) modelling. The contour illustrates the distribution of vertical settlements across the embankment and foundation.

displacement contour obtained from FEM modelling. For this method also, RS is calculated using the Equation (3), but in this method, the crest settlement is taken as the vertical displacement of the dam crest computed from the FEM analysis. Following this, the IM-EDP relation is developed using PSDMs. Method 2 will be referred to as M_2 in the following text.

3.2.1. Validation of the numerical model

The numerical model is based on geometry and material properties of a real-world dam project as discussed by Guo, Dias, and Pan (2019), post-earthquake settlement data for the reference dam were not available, making direct empirical calibration infeasible, so the FEM model was validated against 19 documented case histories of medium-sized embankment dams subjected to similar PGA levels as reported by Swaisgood (2003). Figure 4 illustrates that the model accurately reproduces the observed trend of increasing crest settlement with increasing PGA. Agreement with case histories was quantified using RMSE and mean bias (RMSE = 0.051 m, bias = −0.012 m), indicating that the model reproduces observed behaviour with reasonable accuracy. This suggests that FEM results are consistent with observed performance trends, supporting the credibility of the PSDM and fragility curves.

4. Evaluation parameters

This section provides an overview of the evaluation of IMs, emphasising their effectiveness in predicting EDP. With 14 IMs under consideration, the analysis aims to identify the most appropriate IM for EDP prediction for embankment dams, considering the M_1 and M_2 based PSDMs. To determine the optimal IM for embankment dams, five steps are taken: (1) 21 earthquake

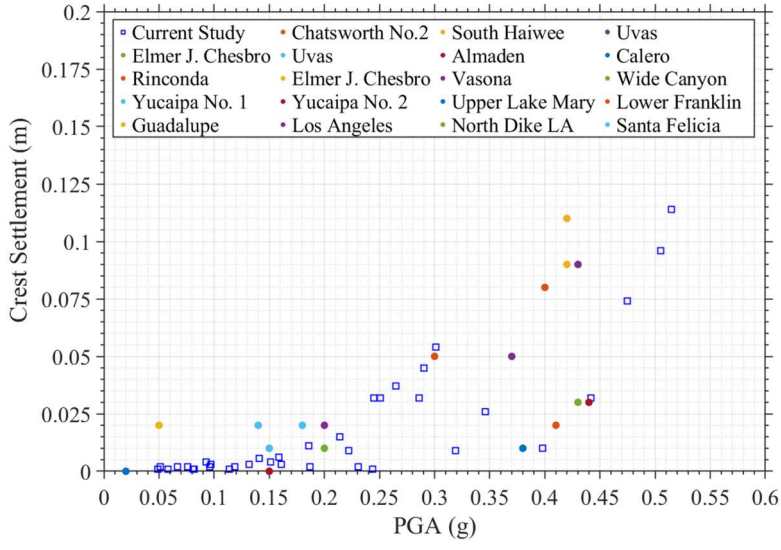

Figure 4. Comparison of crest settlement from the current study with case studies of embankment dams having medium height and subjected to comparable PGA levels as listed by Swaisgood (2003).

records from 11 instrumented embankment dams are selected for empirical analysis (Section 3.1), along with 39 ground motions for numerical simulation (Section 3.2); (2) the acceleration records of these instrumented dams are utilised to assess the accumulated vertical displacement (Section 3.1), and the selected ground motions are input into the developed numerical model to conduct dynamic analysis (Section 3.2); (3) 14 IMs extracted from Step (1) and EDPs obtained from Step (2) are employed for empirical and numerical simulation approaches, respectively, to establish empirical data-based and numerical simulation data-based PSDMs (Section 3); (4) three commonly used metrics for IM evaluation are applied, calculating coefficients for each metric based on both PSDMs: efficiency (Ciampoli and Giovenale 2004), which quantifies the uncertainty of PSDMs (Section 4.1); practicability (Mackie and Stojadinović 2001), which reflects the correlation between IMs and EDPs (Section 4.2); and proficiency (Padgett, Nielson, and DesRoches 2007), which addresses the trade-off between efficiency and practicality (Section 4.3); (5) finally, the coefficients are utilised in the fuzzy comprehensive evaluation method detailed in Section 5 to quantitatively select the optimal IM. The general proposed procedure for optimal IM selection is summarised in Figure 5.

4.1. Efficiency

Efficiency refers to an IM's capacity to predict the corresponding EDP consistently with minimal variability (Ciampoli and Giovenale 2004). In the context of

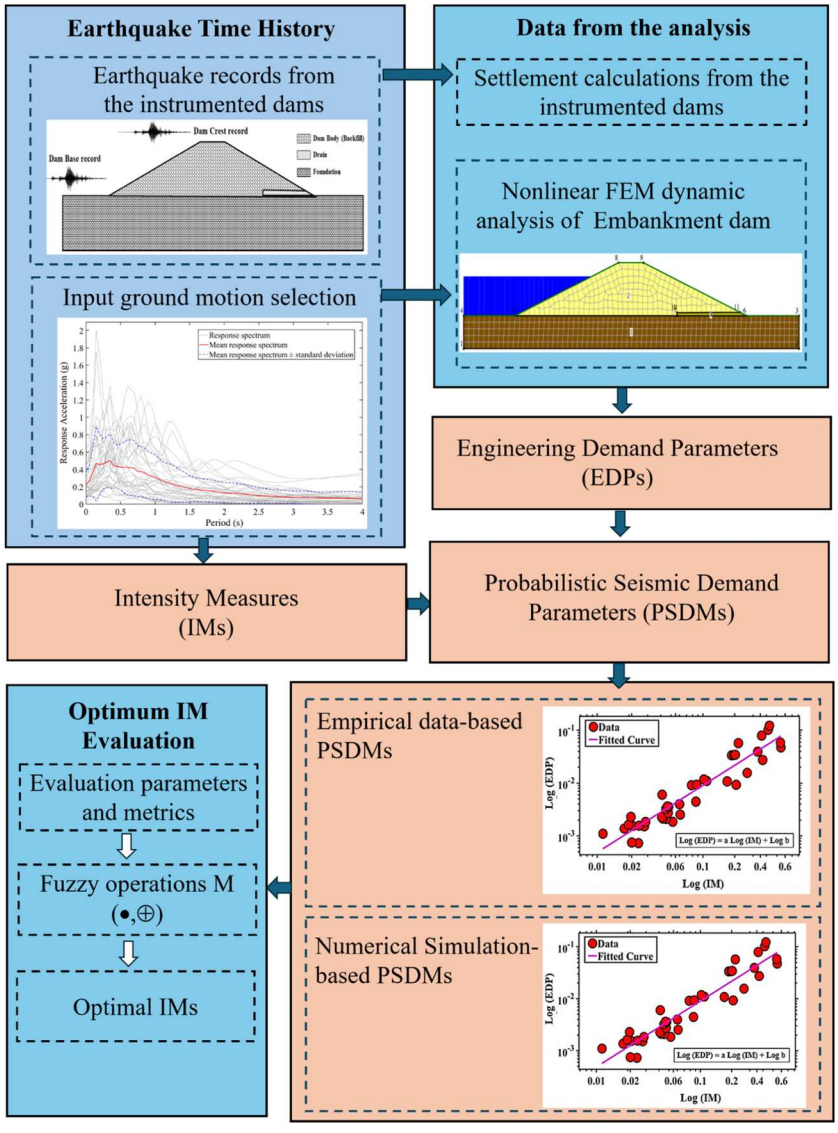

Figure 5. Schematic representation of the proposed framework for evaluating optimal intensity measures (IMs) for embankment dams.

seismic performance assessment, an efficient IM demonstrates a robust and stable correlation with the EDP across diverse ground motions, thereby minimising uncertainty in predicting structural responses. Typically, efficiency is assessed using statistical indicators such as the standard deviation of residuals ($\sigma_{EDP|IM}$), the coefficient of determination (R^2), root mean square error (RMSE), and the correlation coefficient (r).

4.1.1. Correlation coefficients

Pearson correlation coefficients, as discussed by Pinzón et al. (2023), were used here to assess the correlation between the IMs and EDPs. The Pearson coefficient measures the linear relationship between two variables. The Pearson correlation coefficient "r" is defined as the covariance of the two variables divided by the product of their standard deviations σ and is given by Equation (5).

$$r = \frac{Cov(\ln(x_j),\ \ln(y))}{\sigma_{\ln(x_j)}\sigma_{\ln(y)}} \tag{5}$$

where $\ln(x_j)$ and $\ln(y)$ are the natural logarithms of the IM and EDP values, respectively. The term Cov $(\ln(x_j), \ln(y))$ represents the covariance between the two logarithmic variables, while $\sigma_{\ln(x_j)}$ and $\sigma_{\ln(y)}$ are their corresponding standard deviations. A correlation coefficient value close to 1 indicates a strong positive correlation, while a value nearing −1 signifies a strong negative correlation. A coefficient of zero implies no correlation at all.

Figure 6(a) shows that in the Pearson correlation model, PGV, VRMS, AI, CAV, and SMV demonstrate the strongest correlation with the EDP in M_1 and M_2. As a result, PGV, VRMS, AI, CAV, and SMV are the IMs having the best correlation with EDP.

4.1.2. Goodness of fit

The goodness of fit is a widely recognised and effective metric for evaluating data fitting. The linear regression coefficient (R^2) serves as the primary measure of goodness of fit, indicating the extent of deviation between the observed data and the fitted regression line. These regression coefficient values range from 0 to 1, with values closer to 1 reflecting a more accurate representation of the data trend and reduced scatter.

A goodness-of-fit value approaching one indicates a stronger correlation between the IM and the EDP. As illustrated in Figure 6(b), the PGV achieved the highest R^2 values of 0.90 for M_1 and M_2. This was followed by the SMV and the VRMS, which recorded R^2 values of 0.90 and 0.89 and 0.94 and 0.72 for M_1 and M_2, respectively. The AI also performed well, with R^2 values of 0.86 and 0.81 for M_1 and M_2. Additionally, the CAV

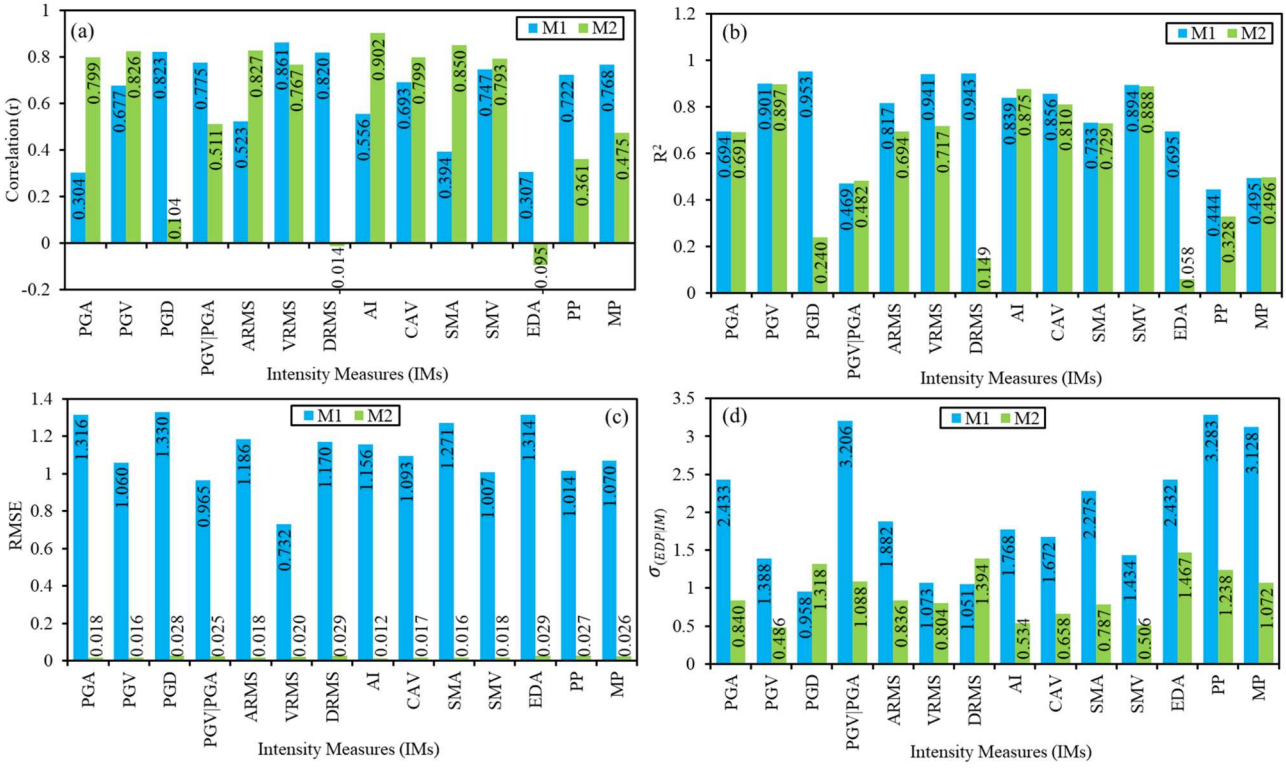

Figure 6. Comparison of: (a) correlation coefficients (r); (b) coefficients of determination (R^2); (c) root-mean-square errors (RMSE); and (d) dispersion ($\sigma_{EDP|IM}$) for each Intensity Measure (IM) obtained using Method 1 (M_1) and Method 2 (M_2).

demonstrated strong performance with R^2 values of 0.85 and 0.81 for M_1 and M_2, respectively. In contrast, PGA, PP, MP, EDA, and PGV|PGA exhibited relatively lower R^2 values. Hence, the PGV, SMV, VRMS, AI, and CAV are better IMs than the others in terms of goodness of fit.

4.1.3. Root Mean Square Error (RMSE)

Root Mean Square Error (RMSE) is a key metric used to evaluate the predictive capability of IMs in estimating the corresponding EDPs. It measures the average magnitude of the prediction error, providing a direct assessment of how closely the predicted EDP values (obtained through regression analysis) from PSDMs obtained from M_1 and M_2 match the actual observed values. RMSE is calculated using Equation (6).

$$RMSE = \sqrt{\frac{1}{n}\sum_{i=1}^{n}(y_i - \widehat{y}_i)^2} \tag{6}$$

where y_i is the observed EDP value, $\widehat{y}_i$ is the predicted EDP value from the model, and n is the number of data points. A lower RMSE implies a more accurate and reliable IM, suggesting smaller deviations between observed and predicted EDPs. From Figure 6(c), we can see that VRMS has the lowest RMSE (0.73), followed by PGV|PGA (0.97), and SMV (1), while PGA has the highest RMSE (1.32) from M_1. Similarly, AI has the lowest RMSE (0.012), followed by PGV (0.016) and SMA (0.016), while DRMS has the highest RMSE (0.029) from M_2.

4.1.4. Standard deviation of residuals (dispersion)

An efficient IM reduces the variation and dispersion of seismic demand predictions for a given ground motion (Ciampoli and Giovenale 2004). M_1 and M_2 PSDMs are employed to evaluate IM efficiency through the standard deviation ($\sigma_{EDP|IM}$), expressed in Equation (7).

$$\sigma_{EDP|IM} = \sqrt{\frac{\sum(\ln EDP_{actual} - \ln EDP_{predicted})^2}{N-2}} \tag{7}$$

where N is the total number of observations for a particular category of $\sigma_{EDP|IM}$, EDP_{actual} is the actual value of EDP from the dataset, and $EDP_{predicted}$ is the value obtained from the fitted curve after putting in the IM value. Efficiency is inversely related to the standard deviation ($\sigma_{EDP|IM}$),a lower efficiency corresponds to a higher standard deviation. The dispersion of various IMs is calculated using Equation (7). A lower value of $\sigma_{EDP|IM}$ indicates a more effective IM, whereas higher values signify reduced efficiency.

As shown in Figure 6(d), PGV has the lowest dispersion, with $\sigma_{EDP|IM}$ values of 1.39 and 0.49 for M_2 and M_1, respectively. Following PGV, SMV ($\sigma_{EDP|IM}$ = 1.43 and 0.51 from M_1 and M_2 respectively), VRMS ($\sigma_{EDP|IM}$ = 1.07 and 0.80 from M_1 and M_2 respectively). AI ($\sigma_{EDP|IM}$ = 1.8 and 0.53 from M_1 and M_2) and CAV ($\sigma_{EDP|IM}$ = 1.67 and 0.65 from M_1 and M_2 respectively) exhibit notable lower dispersion. In contrast, the highest $\sigma_{EDP|IM}$ is observed for the PP ($\sigma_{EDP|IM}$ = 3.28 and 1.23 from M_1 and M_2), indicating that this IM has the highest dispersion. This is followed by EDA ($\sigma_{EDP|IM}$ = 2.43 and 1.47 from M_1 and M_2), PGV|PGA ($\sigma_{EDP|IM}$ = 3.01 and 1.09 from M_1 and M_2), and MP ($\sigma_{EDP|IM}$ = 3.1 and 1.07 from M_1 and M_2).

In summary, the optimal ranking of IMs for efficiency, based on r, RMSE, R^2, and $\sigma_{EDP|IM}$ consistently identifies PGV, SMV, VRMS, CAV, and AI as the most efficient choices for embankment dams.

4.2. Practicality

The practicality criterion directly links the IM and the resulting EDP. When deemed impractical, the EDP shows little to no relationship with the seismic IM magnitude. An IM-EDP relationship is seen as practical if it can be easily constructed from available ground motion IM and nonlinear analysis response values and if it makes sense from an engineering perspective (Ciampoli and Giovenale 2004; Mackie and Stojadinović 2001).

The practicality of an IM is assessed using the coefficient (b), which represents the slope of the regression line, as illustrated in Equation (2). A lower (b) value indicates that the IM has a minimal impact on seismic demand estimation, suggesting impracticality. In contrast, a higher (b) value signifies a more practical IM. Figure 7(a) demonstrates the practicality of various IMs. SMA measure achieved the highest (b) values of 2.47 and 1.9 for M_1 and M_2, respectively, establishing it as the most practical IM. Additionally, PGA and PGV|PGA showed significant practicality, with (b) values of 2.57 and 1.84 and 5 and 1.5 for M_1 and M_2, respectively. CAV (2.30 and 1.33 from M_1 and M_2), PGV (2.5 and 1.29), and SMV (2.15 and 1.32) also demonstrated considerable practicality. In contrast, DRMS exhibited the lowest coefficient (b) values of 1.11 and 0.31 for M_1 and M_2, indicating impracticality. Other IMs with lower practicality include PGD, which had (b) values of 1.26 and 0.46 from M_1 and M_2.

4.3. Proficiency

Proficiency is a criterion that benefits from the simultaneous consideration of efficiency and practicality (Ciampoli and Giovenale 2004; Padgett, Nielson, and DesRoches 2007). A more proficient IM exhibits

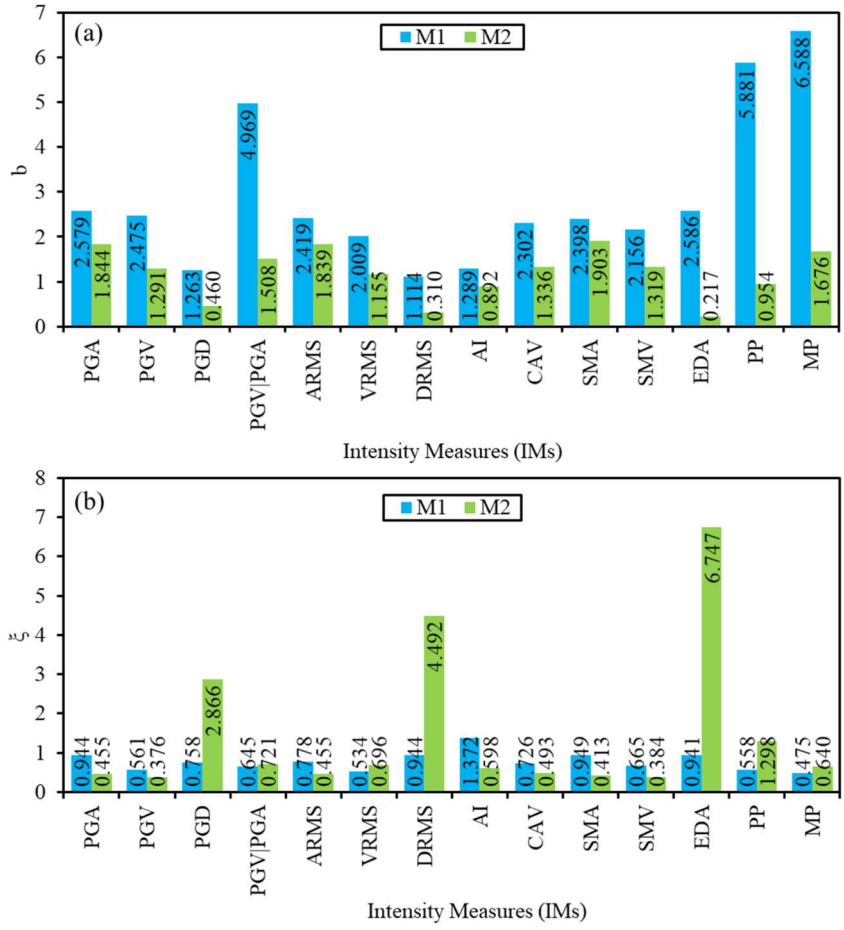

Figure 7. Comparison of: (a) b values for each Intensity Measure (IM) under the practicality criterion; (b) ξ values for each Intensity Measure (IM) under the proficiency criterion, obtained using Method 1 (M_1) and Method 2 (M_2).

reduced, modified dispersion, which underscores the extent of demand uncertainty linked to the choice of IM. Modified dispersion (ξ), derived from Equation (8), defines proficiency.

$$\xi = \frac{\sigma_{EDP|IM}}{b} \tag{8}$$

A low value of ξ signifies a more effective IM. The proficiencies of the IMs, reflected in lower ξ values, are illustrated in Figure 7(b). Upon examining the IMs for ξ, it is evident that PGV exhibits the lowest value among the other IMs, with ξ values of 0.56 and 0.38 for M_1 and M_2, respectively. Other IMs with notably low modified dispersion values include SMV (ξ = 0.66 and 0.38 from M_1 and M_2), CAV (ξ = 0.72 and 0.49 from M_1 and M_2), and VRMS (ξ = 0.53 and 0.70 from M_1 and M_2). Furthermore, the analysis reveals that DRMS has the highest modified dispersion (ξ = 1.48 and 4.49 from M_1 and M_2), followed by EDA (ξ = 0.94 and 6.74 from M_1 and M_2) and PGD (ξ = 0.75 and 2.87 from M_1 and M_2). Based on the findings regarding optimal IM selection criteria, it is highlighted that PGV, SMV, VRMS, CAV, and SMA have the highest proficiency. In contrast, PGA, PGV|PGA, ARMS, AI, and PGD moderately correlate with the EDP. Conversely, DRMS, EDA, PP, and PGV|PGA demonstrate the least proficiency.

Based on the three evaluation parameters leading to six evaluation metrics as discussed above, the top five IMs from M_1 are presented in Table 5, while those from M_2 are shown in Table 6. The data clearly shows notable differences in IM rankings across the six evaluation metrics. From Table 5, it is evident that VRMS,

Table 5. Ranking of intensity measures (IMs) according to evaluation parameters for Method 1 (M_1) (Common IM given in bold).

Evaluation parameters	Metrics	Rank 1	2	3	4	5
Efficiency	r	**SMV**	**PGV**	**VRMS**	CAV	AI
	R^2	PGD	DRMS	**VRMS**	**PGV**	**SMV**
	RMSE	**VRMS**	PGV|PGA	**SMV**	PP	**PGV**
	$\sigma_{EDP\|IM}$	PGD	DRMS	**VRMS**	**PGV**	**SMV**
Practicality	b	MP	PP	EDA	PGA	**PGV**
Proficiency	ξ	MP	**VRMS**	**PGV**	PP	**SMV**

Table 6. Ranking of intensity measures (IMs) according to evaluation parameters for Method 2 (M_2) (Common IM given in bold).

		Rank				
Evaluation parameters	Metrics	1	2	3	4	5
Efficiency	r	**PGV**	**SMV**	**AI**	**CAV**	**VRMS**
	R^2	**PGV**	**SMV**	**AI**	**CAV**	**VRMS**
	RMSE	**AI**	**PGV**	SMA	**CAV**	**SMV**
	$\sigma_{EDP\|IM}$	**PGV**	**SMV**	**AI**	**CAV**	**VRMS**
Practicality	b	SMA	PGA	ARMS	MP	**CAV**
Proficiency	ξ	**PGV**	**SMV**	SMA	ARMS	**CAV**

PGV, and SMV occurred in the top five IMs in efficiency evaluation metrics, but the rank of these IMs is not consistent across metrics (r, RMSE, R^2, and $\sigma_{EDP|IM}$). Furthermore, in practicality evaluation (b), only PGV occurs in the top five, whereas in proficiency evaluation (ξ), VRMS, PGV, and SMV are again occurring, but their order is not consistent. Similarly, Table 6 shows that PGV, SMV, AI, CAV, and VRMS are the IMs that occur in the top five IMs in efficiency evaluations (r, RMSE, R^2, and $\sigma_{EDP|IM}$) but the ranking of these IMs is not consistent in the practicality (b) and proficiency evaluations (ξ). Notably, a specific IM did not achieve a consistent ranking across all parameters, highlighting the necessity of establishing a methodology that can quantitatively integrate and standardise IM performance across different criteria. As a result, we devised a fuzzy comprehensive evaluation framework aimed at quantitatively identifying the optimal IMs, enabling a detailed exploration of the seismic fragility of embankment dams.

5. Proposed fuzzy evaluation framework for ranking intensity measures

The fuzzy comprehensive evaluation method, based on the theory of fuzzy relation synthesis, converts qualitative factors into quantitative metrics for a thorough evaluation. This technique has been widely utilised in both risk assessment and decision-making procedures (Tang et al. 2022; Wang, Shafieezadeh, and Ye 2017; Zhang et al. 2024). We use the fuzzy comprehensive evaluation approach to quantitatively consolidate and balance the performance of IMs across different criteria, allowing for the identification of the most appropriate IM for Embankment Dams. The methodology comprises a combination of performance metric calculations (described in Section 4) and fuzzy logic-based aggregation to produce a single score that indicates the overall effectiveness of each IM. The comprehensive evaluation process applied in this method is illustrated in Figure 8. The procedure for identifying the optimal IM using the fuzzy comprehensive evaluation technique includes:

Step 1: Construction of Factor set and Evaluation set

In the initial phase of evaluating IMs, it is essential to identify and define the relevant evaluation criteria, collectively referred to as the factor set. This factor set encompasses all the attributes that contribute to the overall assessment of IM performance (Tan, Lu, and Zhang 2016; Xin et al. 2021). Formally, the factor set is represented as:

$$U = [U_1, U_2, \ldots, U_m] \tag{9}$$

where U_i denotes the i^{th} evaluation factor and m is the total number of factors considered. For improved interpretability and structured evaluation, the factors are organised hierarchically into two levels:

(1) The primary factor set U_1, which contains high-level qualitative criteria capturing the key dimensions of IM performance, is expressed as:

$$\begin{aligned} U_1 &= [U_{11}, U_{12}, U_{13}] \\ &= [Efficiency, Proficiency, Practicality] \end{aligned} \tag{10}$$

(2) The secondary factor set U_2, which consists of corresponding quantitative metrics that characterise each primary criterion more precisely derived and discussed in section 4 and is shown in Equation (11).

$$\begin{aligned} U_2 &= [U_{21}, U_{22}, U_{23}, U_{24}, U_{25}, U_{26}] \\ &= [\sigma_{EDP|IM}, R^2, RMSE, r, \xi, b] \end{aligned} \tag{11}$$

The evaluation set, V, reflects the outcomes considering the advantages and disadvantages of each evaluation factor:

$$V = [V_1, V_2, \cdots, V_m] \tag{12}$$

where V_i represents a potential comprehensive evaluation outcome. As this study only requires calculating the relative rankings among IMs and not classifying them into distinct levels, the evaluation set is replaced by the rankings among IMs.

Step 2: Construction of the Fuzzy Relation Matrix

To quantitatively express the degree to which each IM satisfies the evaluation criteria, a fuzzy relation matrix is constructed. Each element r_{ij} of this matrix represents the normalised membership degree of the j^{th} IM concerning the ith evaluation factor. Normalisation is achieved using the sum-normalisation method (Tang et al. 2022) in which each raw factor value x_{ij} is

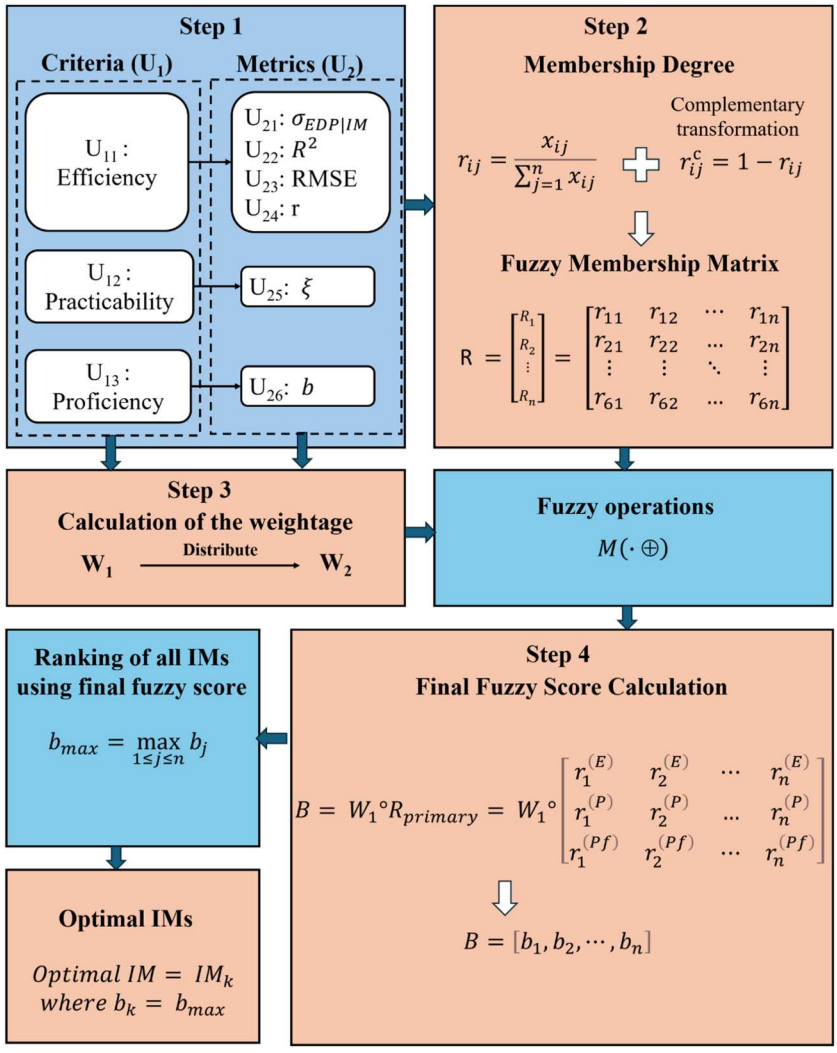

Figure 8. Flowchart of the proposed fuzzy evaluation method for ranking Intensity Measures (IMs).

divided by the total of that factor across all IMs:

$$r_{ij} = \frac{x_{ij}}{\sum_{j=1}^{n} x_{ij}}, \; i = 1, \ldots, m \, ; j = 1, \ldots, n \qquad (13)$$

Where x_{ij} is the raw value of the i^{th} evaluation factor for the j^{th} IM, m is the number of factors, and n is the number of IMs. For factors where, lower values indicate better performance (inverse relationship), such as $\sigma_{EDP|IM}$, RMSE, and ξ, the membership degree is transformed using Equation (14) to its complement to maintain a consistent membership scale where higher values indicate better performance, for inverse factors $i \in \{\sigma_{EDP|IM}, \text{RMSE}, \xi\}$.

$$r_{ij}^{c} = 1 - \frac{x_{ij}}{\sum_{j=1}^{n} x_{ij}}, \; i = 1, \ldots, m \, ; j = 1, \ldots, n \qquad (14)$$

where x_{ij} is the member that requires processing by the complement operation method. This formulation ensures that the normalised values for each metric sum to unity, preserves relative magnitudes, and yields values bounded by [0, 1] when $x_{ij} \geq 0$ for i^{th} evaluation factor (Hwang and Yoon 1981; Tang et al. 2022). Sum-normalisation was employed instead of z-score or min–max scaling, as it avoids the extreme rescaling associated with dependence on a single minimum or maximum value, maintains proportional relationships among the original scores, and provides bounded membership degrees suitable for fuzzy aggregation and weighted combination (Hwang and Yoon 1981; Tang et al. 2022). This normalisation method has also been widely implemented in previous studies (Tang et al. 2022; Zhang et al. 2024). The resulting fuzzy relation matrix aggregates these membership degrees:

$$R = [r_{ij}] = \begin{bmatrix} r_{11} & r_{12} & \cdots & r_{1n} \\ r_{21} & r_{22} & \ldots & r_{2n} \\ \vdots & \vdots & \ddots & \vdots \\ r_{61} & r_{62} & \ldots & r_{6n} \end{bmatrix} \qquad (15)$$

Step 3: Determination of Weight Vector

The weight vector W describes the significance of each evaluation factor. Assigning appropriate weights to the evaluation factors reflects their relative importance in the final assessment.

$$W = [w_1, w_2 \ldots, w_m] \tag{16}$$

where w_i represents the degree of membership for each evaluation factor within U. The weight vectors W_1 and W_2 correspond to the primary factor set (U_1) and the secondary factor set (U_2), respectively. For the primary factor set U_1, the assigned weights are $W_1 = [0.50, 0.25, 0.25]$. Among the three criteria, efficiency is given the highest weight (0.50), while practicality and proficiency share equal weights (0.25 each). This weighting reflects the established consensus that efficiency is the most critical factor in defining IM–EDP relationships, as it reduces the dispersion ($\sigma_{EDP|IM}$) of EDP predictions (Aquib, Sivasubramonian, and Martin Mai 2022; Giovenale, Allin Cornell, and Esteva 2004; Luco and Allin Cornell 2007; Vargas-Alzate, Hurtado, and Pujades 2021). At the same time, practicality and proficiency are also integral to IM selection. Notably, since proficiency inherently incorporates aspects of both efficiency and practicality (Equation 8), prioritising efficiency indirectly enhances proficiency without requiring disproportionate emphasis (Khosravikia and Clayton 2019). Accordingly, the chosen weight $W_1 = (0.50,\ 0.25,\ 0.25)$ provides a balanced evaluation in which efficiency receives twice the weight of the other two criteria, while all three factors retain meaningful representation in the overall assessment.

For the secondary factor set U_2, weights are assigned to the individual metrics, $W_2 = [0.125,0.125,0.125,0.125,0.25,0.25]$. Further W_2 was divided into subvectors corresponding to each primary factor, $W_{2,\text{eff}} = [w_1, w_2, w_3, w_4] = [0.125, 0.125, 0.125, 0.125]$; $W_{2,\text{prac}} = [w_5] = [0.25]$; $W_{2,\text{prof}} = [w_6] = [0.25]$ respectively for efficiency, practicality, and proficiency metrics.

Step 4: Aggregation and Final Fuzzy Scores

5.1. Aggregation of secondary factors into primary factors

To reconcile the secondary factors with the primary qualitative criteria, the secondary factors are aggregated by weighted summation. Specifically, for each j^{th} IM, the membership degree for each primary factor is computed as follows:

$$\begin{cases} r_j^{(E)} = \sum_{k=1}^{4} W_{2,eff} \cdot r_{kj}, \ \textit{Efficiency} \\ r_j^{(P)} = W_{2,prac} \cdot r_{5j}, \ \textit{Practicality} \\ r_j^{(Pf)} = W_{2,prof} \cdot r_{6j}, \ \textit{Proficiency} \end{cases} \tag{17}$$

where $r_j^{(E)}$, $r_j^{(P)}$, $r_j^{(Pf)}$ is aggregated efficiency, practicality and proficiency score for j^{th} IM respectively.w_{2k} is weight for the k^{th} secondary metric. r_{kj} is normalised score of j^{th} IM on secondary factor k. This yields the primary factor membership matrix as shown in Equation (18).

$$R_{primary} = \begin{bmatrix} r_1^{(E)} & r_2^{(E)} & \cdots & r_n^{(E)} \\ r_1^{(P)} & r_2^{(P)} & \cdots & r_n^{(P)} \\ r_1^{(Pf)} & r_2^{(Pf)} & \cdots & r_n^{(Pf)} \end{bmatrix} \tag{18}$$

5.2. Final fuzzy scores and optimal IM selection

The ultimate fuzzy evaluation score for each IM is obtained by the weighted summation of the primary factor memberships with the corresponding weights (Xue and Yang 2014):

$$B = W_1^{\circ} R_{primary} = W_1^{\circ} \begin{bmatrix} r_1^{(E)} & r_2^{(E)} & \cdots & r_n^{(E)} \\ r_1^{(P)} & r_2^{(P)} & \cdots & r_n^{(P)} \\ r_1^{(Pf)} & r_2^{(Pf)} & \cdots & r_n^{(Pf)} \end{bmatrix} = [b_1, b_2, \cdots, b_n] \tag{19}$$

where ○ symbolises the fuzzy operations, and b_i is the degree of membership associated with each evaluation criterion. The score b_j represents the comprehensive fuzzy evaluation for the j^{th} IM and is given by Equation (20).

$$b_j = \sum_{i=1}^{3} W_{1i} r_j^{(i)} = 0.5 r_j^{(E)} + 0.25 r_j^{(P)} + 0.25 r_j^{(Pf)} \tag{20}$$

where b_j is the final aggregated score for the j^{th} IM. In this study, IM rankings are determined by the principle of the maximum membership degree, denoted as b_{max}, the optimal IM is identified by selecting the one with the maximum fuzzy score, signifying it as the most efficient, proficient, and practical predictor of the EDP.

$$b_{max} = \max_{1 \le j \le n} b_j \tag{21}$$

$$\textit{Optimal IM} = V_k, \ \textit{where } b_k = b_{max} \tag{22}$$

where b_{max} is the maximum final score across all IMs, the IM, V_k corresponding to this score is selected as

the optimal IM. The comprehensive evaluation results for the maximum b_{max} related to the optimal IM, with RS as the EDP, are summarised in Figure 9. The top two IMs identified from M_1 are VRMS and PGV which have b_{max} values of 0.1927 and 0.1909, respectively. In contrast, the top 2 IMs from M_2 include PGV and SMV with b_{max} values of 0.1983 and 0.1979 respectively. Notably, PGV appears in the top two for both methods, while VRMS is exclusive to M_1. Consequently, for embankment dams, PGV and VRMS have been selected as the optimal IMs if we take M_1 and M_2 combined. According to Giovenale, Allin Cornell, and Esteva (2004), "hazard computability" refers to the ability to compute seismic risk using current ground motion attenuation relationships. Among the top two optimal IMs (VRMS and PGV from M_1 and PGV and SMV from M_2) obtained in this study, only the attenuation model for PGV has been developed (Bahrampouri, Rodriguez-Marek, and Green 2020; Danciu and Tselentis 2007; Tao et al. 2024), allowing for calculations at specific sites and meeting the criteria for hazard computability.

5.3. Sensitivity analysis of primary factor weights

To evaluate the robustness of IM rankings with respect to variability in the primary factor weights (W_1), a Monte Carlo (MC) sensitivity analysis was performed (Broekhuizen et al. 2015; Mazurek and Strzałka 2022; Więckowski and Sałabun 2023). This analysis quantifies how perturbations in the primary weight vector W_1 = [0.5,0.25,0.25] affect the fuzzy comprehensive scores b_j (Equation 20) and, consequently, the ordinal ranking of IMs under both PSDM methods.

The baseline weight vector is defined as W_1^{base} = [0.5, 0.25, 0.25], in which $w_1^{base} = 0.5$ corresponds to efficiency, $w_2^{base} = 0.25$ to practicality, and $w_3^{base} = 0.25$ to proficiency. For each MC trial t = 1, … , N and each factor k = 1,2,3, an independent standard normal variable is drawn as shown in Equation (23).

$$\epsilon_{t,k} \sim N(0, 1) \tag{23}$$

where $\varepsilon_{t,k}$ represents the gaussian noise term associated with factor k in trial t. These samples are used to generate multiplicative lognormal perturbations given in Equation (24).

$$\eta_{t,k} = e^{(\sigma_{ln} \cdot \epsilon_{t,k})}, \qquad \log \eta_{t,k} \sim N(0, \sigma_{ln}^2) \tag{24}$$

where $\eta_{t,k}$ is the multiplicative noise factor applied to the baseline weight w_k^{base} and σ_{ln} is the standard deviation controlling the typical magnitude of the perturbation (Mazurek and Strzałka 2022). The lognormal perturbation ensures strictly positive weights and multiplicative variation, which is more realistic than additive noise, as negative weights are not meaningful (Limpert, Stahel, and Abbt 2001; Mazurek and Strzałka 2022). The unnormalised perturbed weights are:

$$\hat{w}_{t,k} = w_k^{base} \cdot \eta_{t,k} \tag{25}$$

where $\hat{w}_{t,k}$ is the perturbed weight for factor k in trial t before normalisation. The normalised perturbed weight

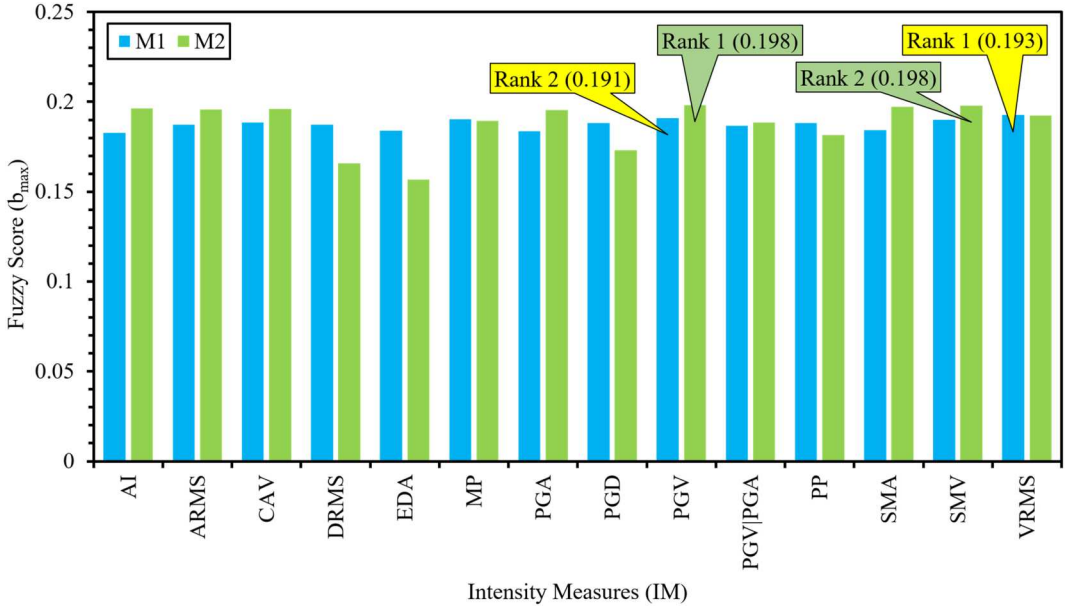

Figure 9. Comparison of fuzzy score (b_{max}) values for 14 intensity measures (IMs) obtained using Method 1 (M_1) and Method 2 (M_2). Blue bars represent M_1 results, and green bars represent M_2 results. The figure highlights the highest-ranked (Rank 1) and second-highest-ranked (Rank 2) IMs for each method based on their b_{max} values.

vector is obtained as:

$$w_{t,k}^{*} = \frac{\hat{w}_{t,k}}{\sum_{m=1}^{K} \hat{w}_{t,m}} = \frac{w_k^{base} \cdot \eta_{t,k}}{\sum_{m=1}^{K} w_m^{base} \cdot \eta_{t,m}} \quad (26)$$

where $w_{t,k}^{*}$ is the normalised perturbed weight for factor k, and K = 3 is the total number of primary factors. For each trial t, the perturbed weights $W_1^{(t)} = [\ \omega_{eff,t}^{*}, \omega_{prac,t}^{*}, \omega_{prof,t}^{*}]$ were substituted into Equation (20) to obtain new fuzzy scores for each IM:

$$b_j^{(t)} = \omega_{eff,t}^{*} r_j^{(E)} + \omega_{prac,t}^{*}\ r_j^{(P)} + \omega_{prof,t}^{*}\ r_j^{(P_f)} \quad (27)$$

where, $b_j^{(t)}$ is the fuzzy comprehensive score of IM_j in trial t; $r_j^{(E)}$, $r_j^{(P)}$, $r_j^{(P_f)}$ are the efficiency, practicality, and proficiency scores for IM_j. IMs were ranked in descending order of $b_j^{(t)}$ to obtain the perturbed rank vector r_t.

The robustness of IM rankings under perturbed primary weights is quantified using complementary metrics. For each trial t, the mean absolute rank change (Δ_t) is calculated as:

$$\Delta_t = \frac{1}{M} \sum_{j=1}^{M} |r_{t,j} - r_j^{base}| \quad (28)$$

where, $r_{t,j}$ is the rank of IM_j in trial t, r_j^{base} is the baseline rank of IM_j, and M is the total number of IMs. In addition, the Spearman correlation (ρ_t^S) between the baseline rank vector (r_{base}) and the perturbed rank vector (r_t) was also computed:

$$\rho_t^S = corr_{Spearman}(r_{base}, r_t) \quad (29)$$

where $\rho_t^S \in [-1,1]$; values closer to 1 indicate that the relative ordering of IMs is largely preserved. Higher values of ρ_t^S indicate that the relative ordering of IMs is largely preserved under W_1 perturbations. A visual summary of rank variability is presented through rank heat maps. In these maps, row i corresponds to IM_i, column j corresponds to rank j, and the colour intensity represents the number of MC trials in which IM_i received rank j. Formally, the rank frequency matrix F is defined as:

$$F_{i,j} = \sum_{t=1}^{N} 1\{r_{t,i} = j\} \quad (30)$$

where $F_{i,j}$ is the frequency of IM_i attaining rank j, $1\{\cdot\}$ is the indicator function, and N is the total number of MC trials. IMs with highly concentrated distributions indicate stable rankings, while spread-out distributions indicate higher uncertainty. The 5th, 50th (median), and 95th percentile ranks computed for each IM provide an additional quantitative measure of rank uncertainty (Broekhuizen et al. 2015; Więckowski and Sałabun 2023).

$$r_{j,(p)} = Quantile_p\{r_{t,j}\}_{t=1}^{N}\ ,\ p = 5\%, 50\%, 95\% \quad (31)$$

where $r_{j,(p)}$ is the rank of IM_j corresponding to the pth percentile across all MC trials.

The sensitivity analysis was conducted with N = 10,000 MC trials. The results for the baseline case, corresponding to $\sigma_{ln} = 0.15$ ($\approx \pm 15\%$ variability), are shown here. In M_1, Δ_t was 0.557, and a ρ_t^S was 0.969 (median 0.978). IM-specific results show that VRMS remained the top-ranked IM with low variability. For M_2, the results indicate even higher robustness, with Δ_t of 0.148 and a ρ_t^S of 0.991 (median 1). IM-specific results show that PGV remained the top-ranked IM with low variability.

Figure 10 illustrates the average absolute change in fuzzy comprehensive scores resulting from perturbation; both PSDM methods showed a very small change in fuzzy scores ($\approx$ 0.0056–0.0069). In M_1, the largest change (~0.0069) occurs for DRMS, followed by PGD and VRMS, while MP shows the smallest (~0.0056). In M_2, the largest change (~0.007) is observed for AI, followed by SMV and PGV, while MP has the smallest change (~0.0062). The corresponding rank-frequency heatmaps in Figure 11.

The 5th–95th percentile rank intervals in Figure 12 further corroborates this stability. In M_1 most IMs vary by fewer than two rank positions. Top-ranked IM VRMS has a median rank of 1. IMs such as PGA, AI, and SMV display narrow uncertainty bands, whereas DRMS, PP, MP and PGV|PGA exhibit slightly wider intervals of 4–6 ranks. In M_2 again, IM yields more compact intervals, with top rank IM PGV having a median rank of 1, whereas PGA, ARMS, AI, and SMA exhibit slightly wider intervals of 3–4 ranks. Hence, the top-ranked IMs (VRMS from M_1 and PGV from M_2) found relatively insensitive to changes in W_1.

To examine the influence of stronger perturbations, σ_{ln} was increased incrementally from 0.10 to 0.50. In Figure 13, as expected, larger perturbations resulted in slightly higher Δ_t and lower ρ_t^S. In M_1, Δ_t rose from $\approx$ 0.40 to $\approx$ 1, while ρ_t^S decreased from $\approx$ 0.98 to $\approx$ 0.86. In M_2, the Δ_t remained smaller ($\approx$ 0.06 to 1) and ρ_t^S changes only slightly ($\approx$ 0.995 to 0.965). Even at the highest perturbation level (σ_{ln} = 0.50), ρ_t^S remained above 0.85, indicating strong preservation of relative rank order. This indicates that IM rankings remain largely unaffected by approximately ±10–50 % variations in the W_1, thereby demonstrating the robustness of the ranking framework and its ability to consistently preserve the relative ordering of IMs (Limpert,

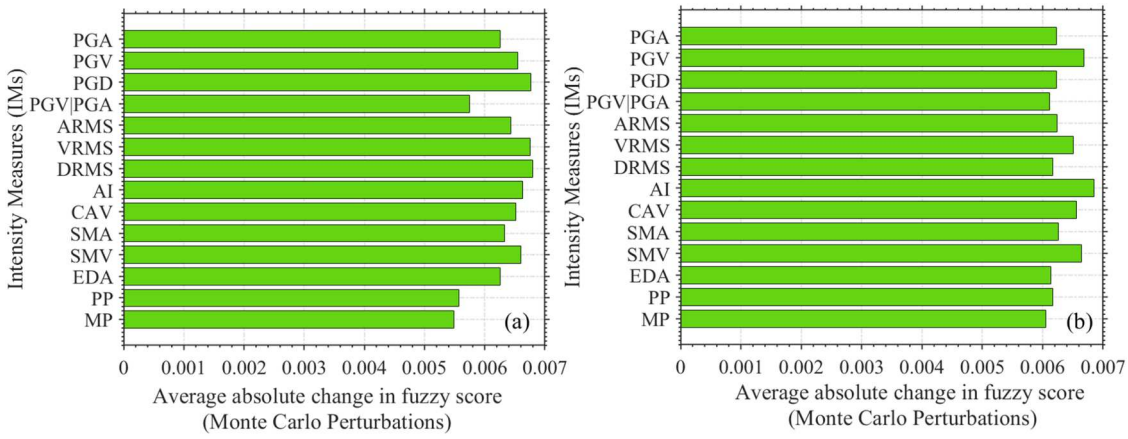

Figure 10. Average absolute change in fuzzy scores for different Intensity Measures (IMs) under Monte Carlo perturbations of the primary factor weights (at $\sigma_{ln} = 0.15$): (a) Method 1; (b) Method 2.

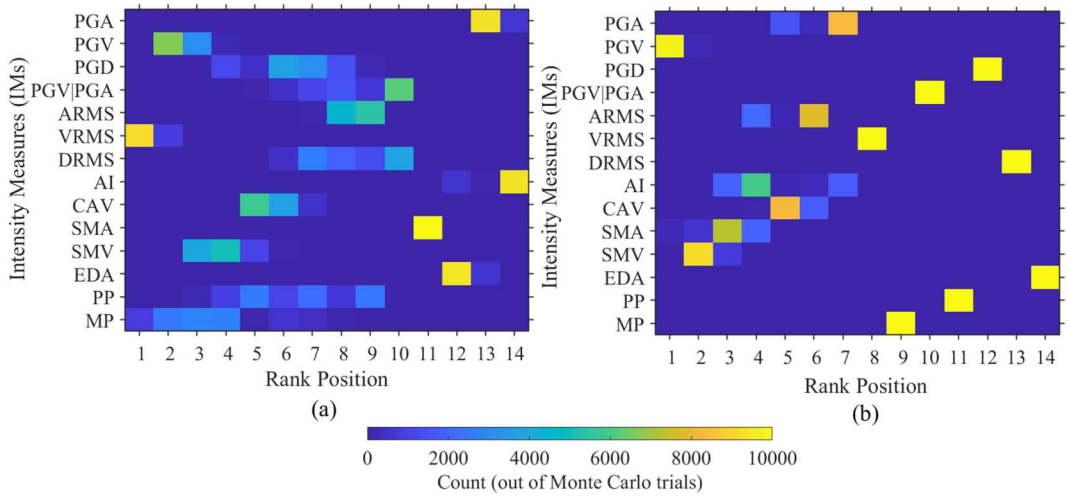

Figure 11. Rank distribution of intensity measures (IMs) under Monte Carlo perturbations of the primary factor weights (at $\sigma_{ln} = 0.15$): (a) Method 1; (b) Method 2. Colour intensity represents the frequency of each IM attaining a given rank position across 10,000 trials. Concentrated yellow bands denote stable ranks, while diffuse blue regions indicate higher variability in ranks.

Stahel, and Abbt 2001; Saltelli et al. 2008; Więckowski and Sałabun 2023).

6. Seismic fragility analysis

Fragility curves provide a quantitative approach to rapidly assess a structure's seismic response. These curves give the likelihood of dams exceeding a specific damage state in response to a given level of ground shaking, influenced by IMs such as PGA or Sa (Hurtado-López and Mayoral-Villa 2019; Rathje and He 2022; Saeidi et al. 2019; Zentner et al. 2011). Conducting a seismic fragility assessment is crucial for evaluating the vulnerability of embankment dams subjected to earthquake loading. This approach follows a probabilistic framework, integrating PSDMs and damage state (DS) thresholds to generate fragility curves that quantify the probability of exceeding different DS levels for varying IMs. The methodology adopted here is consistent with established procedures in recent fragility studies (Khalid et al. 2023; Rathje and He 2022).

6.1. Fragility function

The fragility function expresses the probability that the EDP exceeds a specified DS threshold for a given IM. It is commonly formulated in the EDP domain as in Equation (32) (Khalid et al. 2023; Rathje and He 2022).

$$P(EDP \geq DS|IM) = 1 - \Phi\left(\frac{\ln(DS) - (\ln a + b \ln IM)}{\sqrt{\sigma^2_{\ln EDP} + \sigma^2_{DS}}}\right) \quad (32)$$

where, $P(EDP \geq DS|IM)$ represents the probability of

exceeding a given DS, $\Phi(\cdot)$ is the standard normal cumulative distribution function (CDF), a and b are regression coefficients from the PSDM, $\sigma_{\ln EDP}$ is the dispersion of demand given IM, and σ_{DS} is the uncertainty in the damage state threshold ($DS_{threshold}$) (Cornell et al. 2002; Jalayer and Allin Cornell 2009). The mean $DS_{threshold}$ in log-space is:

$$\mu_{DS} = \ln(DS_{threshold}) \tag{33}$$

Equation (32) can be algebraically rearranged into the IM-domain as:

$$P(EDP \geq DS|IM) = \Phi\left(\frac{\ln(IM) - \mu_{IM|DS}}{\sigma_{IM}}\right) \tag{34}$$

where, $\mu_{IM|DS}$ is the log-median intensity measure capacity associated with a given DS.

$$\mu_{IM|DS} = \frac{\ln(DS_{threshold}) - \ln a}{b} \tag{35}$$

The total uncertainty in the fragility function is expressed by Equation (36).

$$\sigma_{IM} = \frac{\sqrt{\sigma^2_{\ln EDP} + \sigma^2_{DS}}}{b} \tag{36}$$

where, σ_{DS} is the standard deviation reflecting epistemic uncertainty in the DS threshold. Equations (32) and (34) are mathematically equivalent; the latter form is implemented in this study. Similar IM-domain fragility formulations have been presented in prior research (Bakalis and Vamvatsikos 2018; Flenga and Favvata 2021). The residual dispersion σ_{EDP} is estimated from the regression model as:

$$\sigma_{EDP} = \sqrt{\frac{\sum(\ln(EDP_i) - (\ln(a) + b\ln(IM)))^2}{N-2}} \tag{37}$$

where N is the number of ground motion records, ln (EDP_i) is the log-transformed value of the EDP for the i^{th} earthquake record. $ln(a) + b \cdot \ln(IM)$ is the predicted log-transformed EDP value for the i^{th} earthquake record, based on the regression model. The RS functions as the EDP and is calculated using Equation (3), while the IM is obtained from the input motion. As the EDP, the RS captures the vertical impacts of deviatoric sliding deformation, co-seismic volumetric changes, and potential post-liquefaction volumetric recompression. It is assumed that the RS reflects the dam's susceptibility to cracking (He and Rathje 2024).

6.1.1. Damage states

Damage states (DS) serve as key indicators for characterising the seismic response and extent of damage sustained by a structure and should be readily observable or measurable during post-event inspections. In this study, DS are primarily defined using RS, calculated from Equation (3). RS is the most widely adopted EDP in fragility assessments of earthen dams (He and Rathje 2024) because it is dimensionless, straightforward to measure in the field using standard survey techniques, and supported by case histories and empirical guidelines linking settlement magnitude to observed performance (Fell et al. 2005; Pells and Fell 2003; Swaisgood 2003). It was selected as the sole quantitative indicator of DS due to its consistency, reproducibility, and established application in analytical fragility studies (Kwak et al. 2016; Regina et al. 2023). Its primary advantage lies in directly reflecting permanent crest deformation, which is both observable in the field and replicable in numerical simulations.

Although RS is the only metric employed here, it effectively represents a broader, multi-component damage framework: earth dam damage can also manifest through freeboard reduction, global instability, filter displacements, normalised crest settlement (NCS), or Fell damage classes (Regina et al. 2023; Swaisgood 2003). Many of these indicators correlate strongly with crest settlement, and NCS is essentially a normalised form of RS empirically linked to post-earthquake dam performance. By relying on RS, the approach maintains simplicity, reproducibility, and practical applicability, while remaining consistent with established empirical and analytical frameworks for fragility modelling.

For fragility modelling, DS are classified into five levels based on RS: DS1 (Minor: 0.03–0.2%), DS2 (Moderate: 0.2–0.5%), DS3 (Major: 0.5–1.5%), DS4 (Severe: 1.5–5%), and DS5 (Collapse: > 5%). These thresholds follow prior classifications (Swaisgood 2003; Pells and Fell 2003) with a minor modification to omit a separate no/slight category (RS < 0.03%). Similar RS-based classification schemes have also been applied in recent studies (Khalid et al. 2023; Rathje and He 2022).

It is important to note that DS, as defined by RS, correlates with, but is not equivalent to, operational performance levels. Performance levels also consider factors such as functionality, repairability, and residual capacity (Fell et al. 2005; Regina et al. 2023). For decision-making, RS thresholds are mapped to performance categories: DS1–lower DS2 to serviceable conditions; upper DS2–lower DS3 to life-safety or restricted operation; upper DS3– lower DS4 to transition from life-safety to collapse-prevention conditions; and upper DS4–DS5 to collapse-prevention or breach

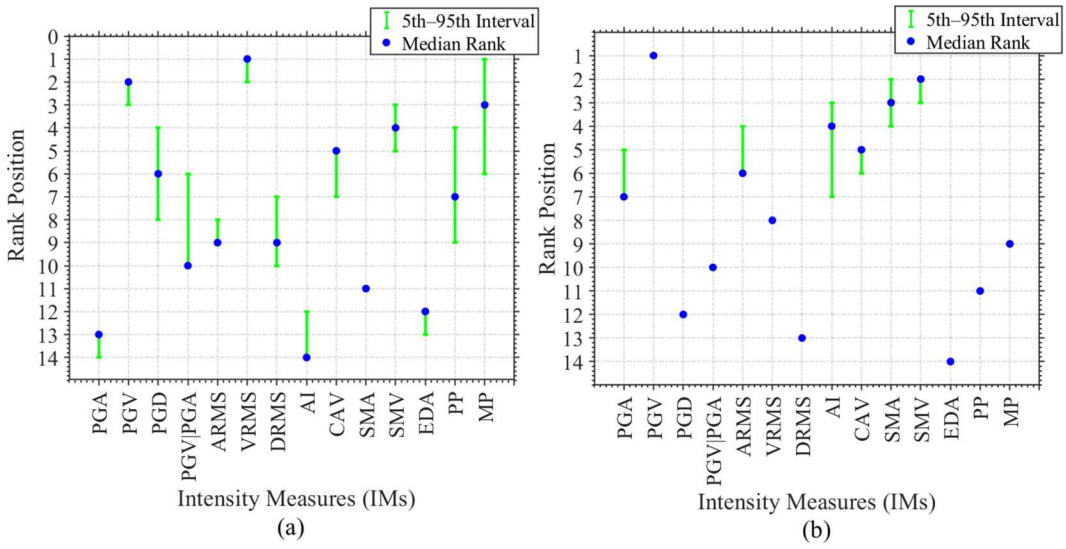

Figure 12. Median rank positions with 5th – 95th percentile intervals for Intensity Measures (IMs) under Monte Carlo perturbations of the primary factor weights ($\sigma_{ln} = 0.15$): (a) Method 1; (b) Method 2.

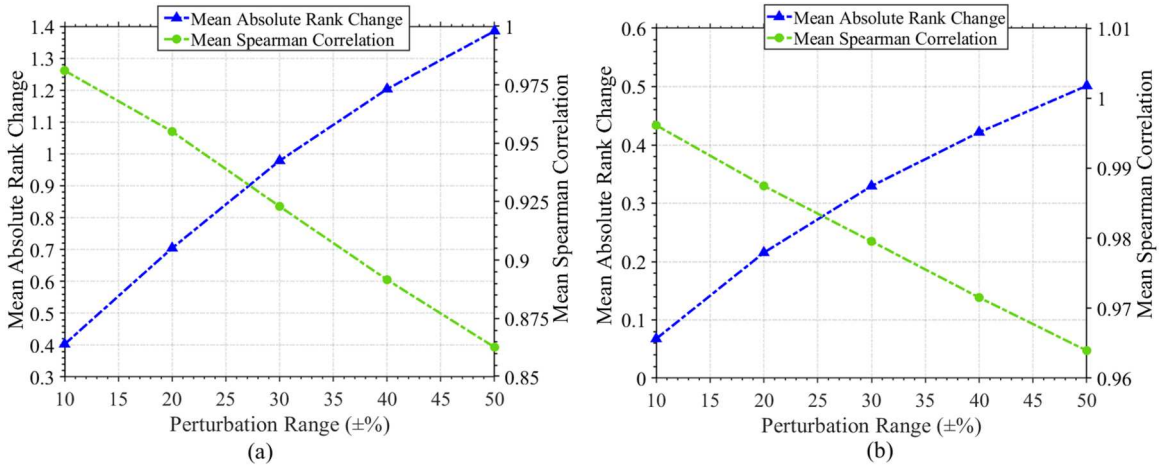

Figure 13. Variation of mean absolute rank change and mean Spearman correlation with increasing perturbation range (±10–50%) of primary factor weights: (a) Method 1; (b) Method 2.

risk. This mapping ensures that RS-based DS definitions convey both the physical extent of deformation and the broader implications for dam safety, functionality, and residual capacity (Fell et al. 2005; Pells and Fell 2003; Regina et al. 2023; Swaisgood 2003).

6.2. Fragility curves

Fragility curves for embankment dams were developed for the optimal IMs using PSDMs from M_1 and M_2. In M_2, scaling ground motion records is crucial for evaluating seismic vulnerability at different ground motion intensities. This process adjusts the IM of the original record to simulate various seismic loading levels. The resulting fragility curves show the probability of exceeding specific DS based on seismic IM, offering insights into damage likelihood under varying earthquake IMs. Figure 14(a,b) illustrates the seismic fragility curves for the top two IMs derived from M_1, while Figure 14(c,d) presents the corresponding curves for the top two IMs from M_2. These curves facilitate a comparison of the failure probabilities associated with each IM. Notably, for the minor damage state (DS = 0.03%), VRMS displays a steeper slope, indicating that even a slight increase in this IM results in a considerably higher probability of exceedance compared to the other two IMs in M_1. Additionally, at very low values (e.g. 0.5) of PGV and SMV, the probability of exceedance has surpassed at least DS1, DS2, DS3, and DS4 in M_2.

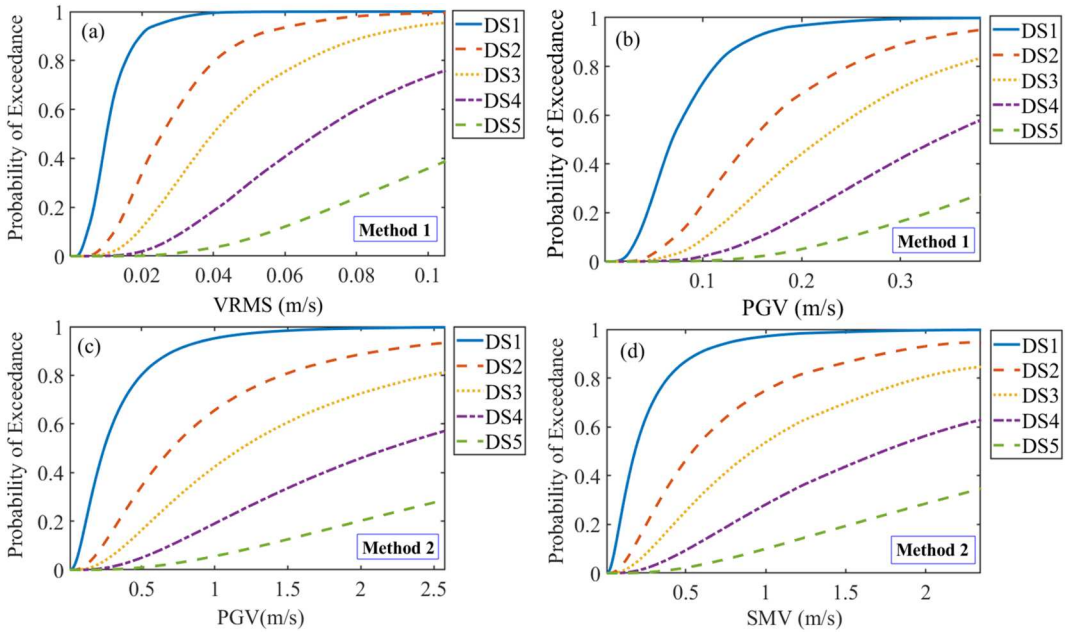

Figure 14. Seismic fragility curves for the top two intensity measures (IMs). Panels (a) and (b) present the fragility functions obtained from Method 1 for VRMS and PGV, respectively, while panels (c) and (d) correspond to Method 2 for PGV and SMV, respectively.

6.2.1. Comparison of fragility outcomes using conventional and optimal intensity measures

To examine the influence of IM selection on seismic fragility estimation, a comparative analysis was conducted between the conventional IM (PGA) and the velocity-based optimal IMs, VRMS (from M_1) and PGV (from M_2). The Figure 15(a–j) illustrate the fragility curves, evaluating the differences in the probability of exceeding each damage state (DS1–DS5). In each case, the PGA-based curve is presented for reference, allowing visual comparison with the curves obtained for the optimal IMs. The results demonstrate that PGA systematically underestimates the probability of exceeding all DS relative to the velocity-based IMs. For VRMS (Figure 15(a,c,e,g,i)), the maximum underestimation by PGA reaches 41% for DS1, 33% for DS2, 28% for DS3, 21% for DS4, and 4% for DS5. For PGV (Figure 15(b,d,f,h,i,j)), the corresponding maximum underestimation is 21% for DS1, 19% for DS2, 15% for DS3, 11% for DS4, and 7% for DS5. These differences quantify the extent to which exclusive use of PGA can underestimate seismic risk. The disparity between PGA and velocity-based IMs fragility curves is most evident for the lower damage states (DS1–DS3). At higher damage states (DS4–DS5), the curves converge as deformation approaches ultimate capacity, although underestimation by PGA remains apparent. The largest discrepancies were observed at 41% for VRMS (M_1, DS1) and 21% for PGV (M_2, DS1).

Across both PSDM frameworks, the velocity-based IMs consistently outperform PGA in predicting damage probability. In the empirical PSDM (M_1), VRMS, which incorporates both amplitude and duration effects, provides a more reliable measure of cumulative damage potential. In the numerical PSDM (M_2), PGV, which represents peak ground velocity and correlates with deformation demands, yields higher exceedance probabilities. These results demonstrate that velocity-based IMs better capture the dominant physical mechanisms governing the seismic response of embankment dams. As shown in the earlier evaluation metrics (Tables 5 and 6), VRMS and PGV exhibit higher correlation coefficients (r, R^2) and lower conditional dispersion ($\sigma_{EDP|IM}$), while PGA is not even in the top 5 IMs. These quantitative metrics support the observed fragility outcomes and confirm that PGA-based fragility models underestimate seismic vulnerability. Overall, the results highlight the importance of selecting optimal IMs, such as VRMS or PGV, that accurately represent the structural response characteristics and site-specific ground-motion conditions.

6.2.2. Comparison of optimal IMs across PSDM methods

The optimal IMs VRMS for the empirical PSDM (M_1) and PGV for the numerical PSDM (M_2) are velocity-based IMs; however, their predictive behaviour can vary due to differences in physical meaning, IM-EDP dataset characteristics, and modelling approach. PGV, representing the peak instantaneous ground velocity, correlates strongly with peak and permanent deformation demands (Khalid et al. 2023; Rathje and He

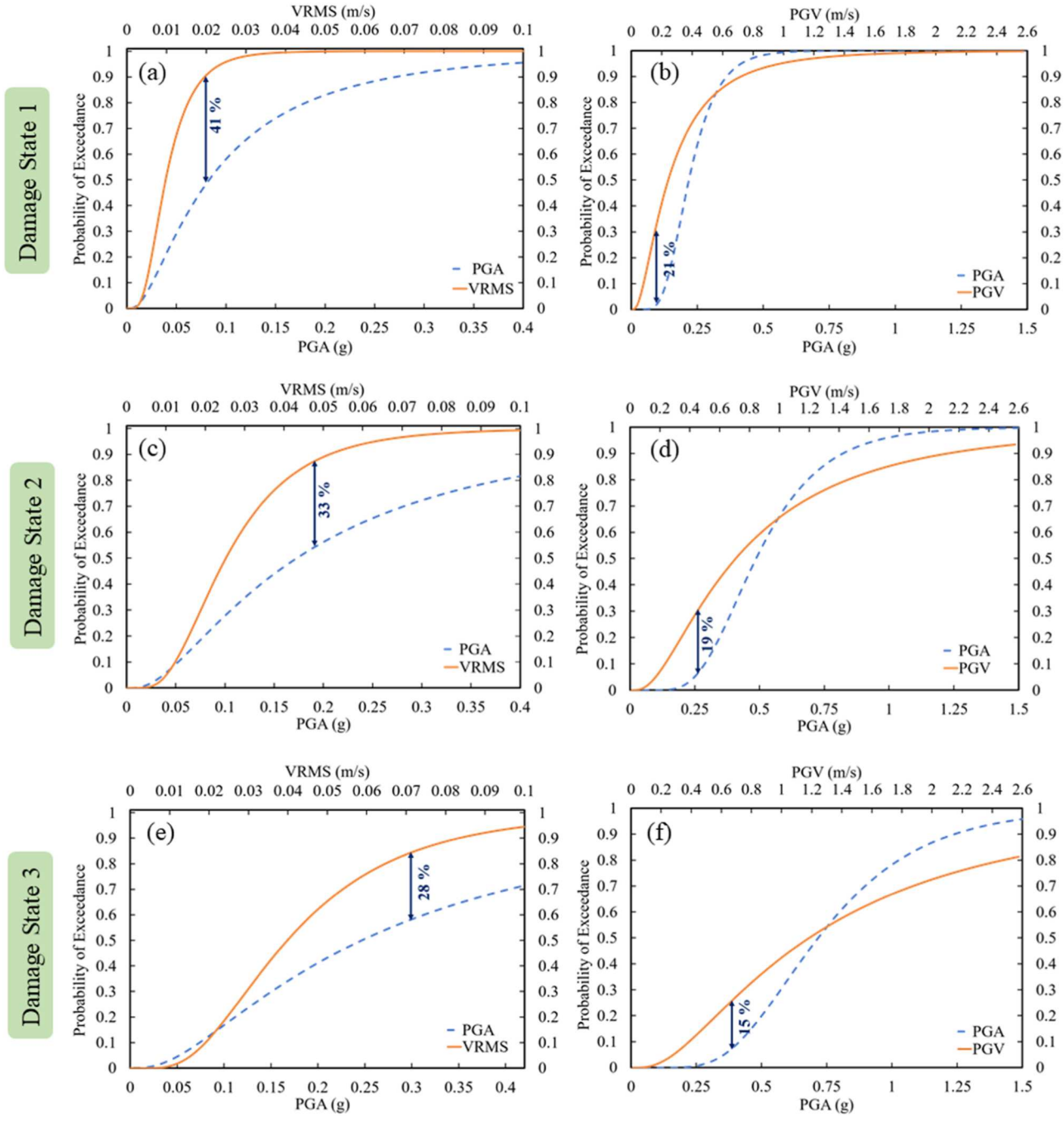

Figure 15. Comparison of fragility curves developed using the conventional intensity measure (PGA) and the optimal IMs (VRMS from Method 1 (M_1) and PGV from Method 2 (M_2)). Panels (a), (c), (e), (g), (i) correspond to M_1 (VRMS), while panels (b), (d), (f), (h), (j) correspond to M_2 (PGV) for DS1–DS5, respectively. Blue lines represent the PGAs, and orange lines represent the optimal IMs. Annotated values indicate percentage-point differences in exceedance probability between IMs at each damage state, quantifying the underestimation associated with PGA.

2022). In contrast, VRMS captures the cumulative velocity energy of ground motion and is therefore more responsive to duration-dependent, energy-related demands (Bray and Travasarou 2007; Luco and Allin Cornell 2007; Rathje and Antonakos 2011).

In M_1, which is based on seismic records from instrumented embankment dams of different heights predominantly subjected to interplate ground motions, the heterogeneous dataset of EDP and IM from different embankment types reflects prolonged shaking and variability in embankment dam types. Under such conditions, where cumulative energy governs deformation, VRMS provides a more representative measure of structural response. Conversely, the numerical PSDM (M_2)

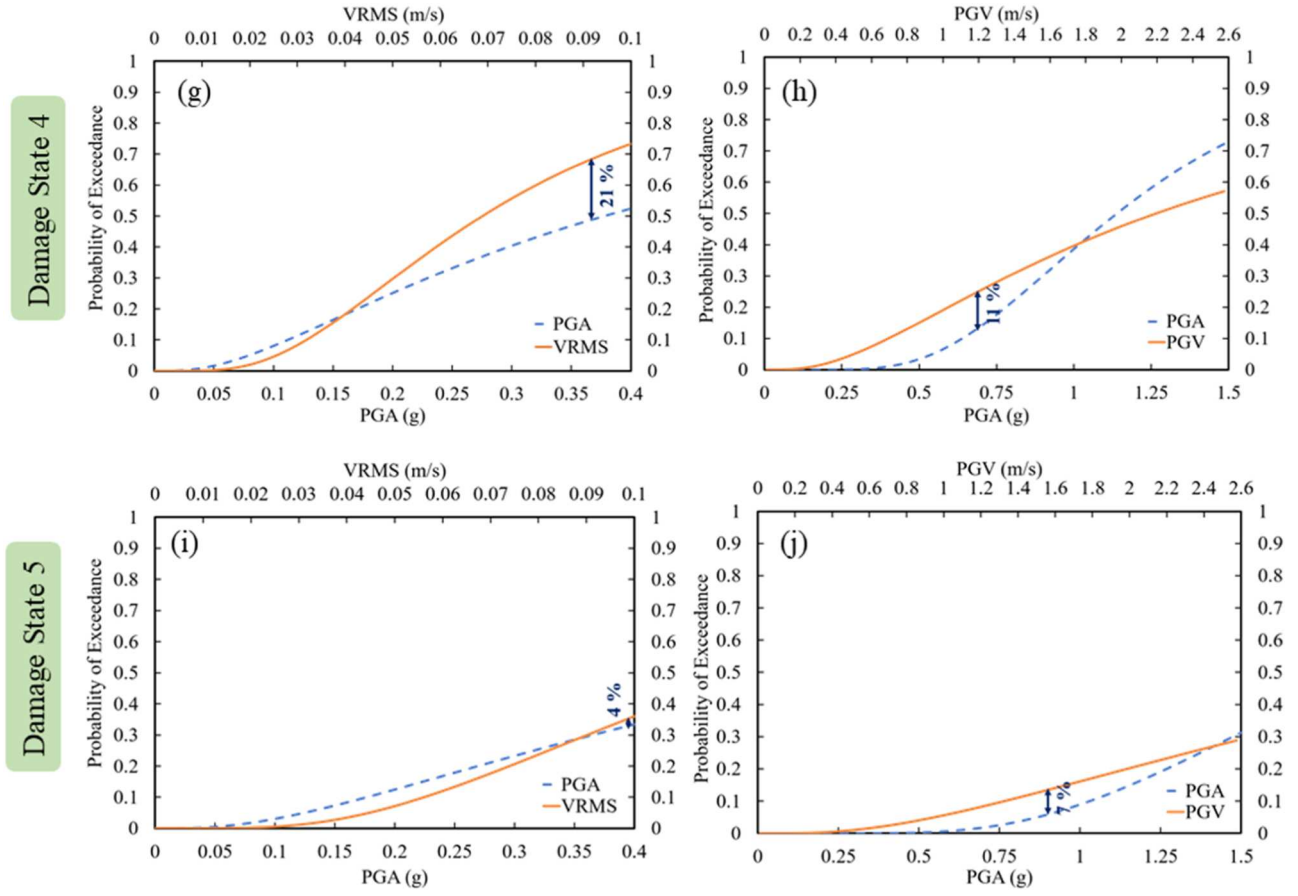

Figure 15. *Continued.*

employs a homogeneous embankment dam FEM model and a comprehensive suite of scaled ground motions encompassing both interplate and intraplate events. The resulting deformations are primarily controlled by peak response amplitudes, for which PGV exhibits a stronger correlation with crest displacement.

The definition of the EDP further supports this difference. In M_1, crest settlement is defined as the accumulated vertical displacement at instrumented points along the crest, emphasising cumulative response. In M_2, it is defined as the average crest displacement along the dam crest, emphasising peak deformation. These differences in EDP definition, combined with the nature of the ground-motion datasets, can account for the selection of distinct optimal IMs. Accordingly, the optimal IMs identified in this study reflect the contrasting characteristics of the two PSDM frameworks: VRMS is better suited for different types of instrumented embankment dams having different heights, whereas PGV is more appropriate for homogeneous dam configurations. Recognising these distinctions ensures that the derived fragility relationships remain physically consistent and representative of embankment-dam seismic performance.

7. Practical implications for seismic design and safety assessment of dams

The results of this study emphasise the need for optimal IMs and dam-specific fragility functions to realistically capture seismic demand, especially for deformation-dominated failure modes. Conditioning fragilities, monitoring thresholds, and design spectra based on PGV and VRMS provide a more representative measure of seismic energy input, consistent with site- and performance-specific guidelines (FEMA 2005; ICOLD 2010).

7.1. Implication for seismic design

Traditional design approaches often rely on PGA or Sa based design spectra; however, this study found that PGA-based fragility curves underestimate the damage probability compared to optimal IMs. So, integrating PGV and VRMS into design spectra can ensure that deformation and associated risk are properly represented. Ground-motion selection and scaling can be adjusted to preserve PGV and VRMS targets, in addition to PGA. Numerical and empirical models can

be calibrated using instrumented embankment dam records (Pells and Fell 2003; USACE 2007; USSD 2022).

7.2. Implication for the safety assessment of existing dams

PGV and VRMS-based fragility curves enable the setting of alarm thresholds, the interpretation of instrumentation data, and the guidance of post-earthquake assessments. Real-time computation of PGV and VRMS from strong-motion and pore-pressure sensors supports rapid post-earthquake assessment and risk-informed operational decisions (USACE 1995). Additionally, velocity-based fragility functions can inform retrofitting strategies aimed at reducing deformation vulnerability. Measures such as slope flattening, downstream buttressing, and reinforcement can be prioritised based on PGV and VRMS-based fragility curves (Aljawhari, Gentile, and Galasso 2022).

7.3. Integration into probabilistic seismic risk assessment

In probabilistic seismic risk assessment, the annual probability of exceeding a DS, denoted ϑ_{ds}, can be obtained by combining the IM hazard with the IM-conditional fragility:

$$\vartheta_{ds} = \int_0^\infty P(DS \geq ds|IM = x)d\lambda_{IM}(x) \qquad (38)$$

where λ_{IM} (x) is the annual frequency of exceeding IM level x. Here, ϑ_{ds} represents the yearly probability that an embankment dam will experience at least the specified DS. Using PGV and VRMS-based fragilities reduces uncertainty for deformation-driven failure modes and provides more credible annual exceedance estimates, supporting performance-based dam safety decisions and the prioritisation of inspections, monitoring, and retrofits (FEMA 2005; ICOLD 2010).

8. Conclusions

The increasing focus on performance-based assessments of multifunctional structures, such as embankment dams, underscores the urgent need to ensure their safety during seismic events. Given their critical roles in water storage and electricity generation, it is essential to enhance methodologies used to evaluate seismic performance. This study examined 14 IMs that influence the seismic vulnerability of embankment dams, classifying them into three categories: three based on frequency, two based on energy, and nine based on amplitude. PSDMs were developed using two distinct approaches: one based on empirical data from historical earthquake records of instrumented embankment dams, and another using numerical simulations with finite element method models subjected to ground motion records from both free-field and dam site stations. A quantitative framework was proposed to identify the optimal IMs for fragility curve development, assessing the optimality of 14 IMs across three criteria: efficiency, practicality, and proficiency. The fuzzy comprehensive evaluation method was subsequently applied to determine the optimal IMs for both empirical and numerical simulation-based PSDMs. Dam damage was classified into five states using relative crest settlement ratio as the engineering demand parameter. The seismic fragility curves were developed using PSDMs from both empirical and numerical data. The key findings of this study are summarised as follows:

- Velocity-based IMs were superior for characterising seismic vulnerability. VRMS was identified as the optimal IM for empirical PSDMs (M_1), while PGV was optimal for numerical PSDMs (M_2), achieving the highest fuzzy evaluation scores. The commonly used IM, PGA, did not satisfy the optimality criteria, while EDA and AI (empirical PSDMs) and EDA and DRMS (numerical PSDMs) were identified as the least effective IMs.
- PGA systematically underestimates the probability of exceeding each defined DS relative to optimal IMs (VRMS and PGV). For VRMS, the maximum underestimation by PGA reaches 41% for DS1, 33% for DS2, 28% for DS3, 21% for DS4, and 4% for DS5. Similarly, for PGV, the maximum underestimation by PGA reaches 21% for DS1, 19% for DS2, 15% for DS3, 11% for DS4, and 7% for DS5. These results indicate that reliance on PGA alone can produce non-conservative predictions of seismic damage.
- Empirical PSDMs captured the variability in seismic responses across multiple instrumented embankment dams of different heights, emphasising duration-sensitive measures like VRMS, whereas numerical PSDMs provided consistent predictions for a homogeneous dam, with PGV preferred for representing peak instantaneous velocity; differences in engineering demand parameters (accumulated vertical displacement for empirical PSDM versus average crest displacement for numerical PSDM) further support selecting VRMS for instrumented embankment dam types of different heights and PGV for homogeneous embankment dam.
- Monte Carlo sensitivity analysis (10,000 trials) results indicate that VRMS and PGV showed minimal changes in fuzzy scores (0.005–0.007), narrow

percentile intervals, and high Spearman correlation coefficients (>0.85) under ±10–50% perturbations of primary criteria weight, indicating robustness against moderate uncertainty.

- Based on these findings, VRMS is recommended as optimal IM for instrumented embankment dams of different types and heights, and PGV for homogeneous embankment dams. Velocity-based IMs provide the most reliable representation of seismic demand, supporting performance-based design, risk-informed safety assessment, and prioritisation of monitoring and retrofitting interventions.

Overall, these findings offer valuable insights into the seismic vulnerability of embankment dams and underscore the need for ongoing enhancements to assessment frameworks to better safeguard these critical structures against potential earthquake impacts. The results of the numerical simulation-based PSDMs (M_2) specifically pertain to homogeneous embankment dams with defined geometrical and geotechnical characteristics; different outcomes may occur for other dam types with varying geometries and mechanical properties.

Acknowledgements

The authors would like to thank the Dam Safety (Rehabilitation) Directorate, Central Water Commission (CWC) for funding the "International Centre of Excellence in Dam Engineering" (ICoEDE) under the Dam Rehabilitation and Improvement Project (DRIP); Ministry of Jal Shakti (MoJS), Government of India for the project entitled "Integrated Investigation for Risk Assessment of the Dam" under grant R-24011/57/2023-Pen Riv Section-MOWR.

Disclosure statement

No potential conflict of interest was reported by the author(s).

Data availability

Some or all data, models, or codes that support the findings of this study are available from the corresponding author upon a reasonable request.

References

Adamo, Nasrat, Nadhir Al-Ansari Nadhir Al-Ansari, Varoujan Sissakian, Jan Laue, and Sven Knutsson. 2020. "Dam Safety: Use of Seismic Monitoring Instrumentation in Dams." *Journal of Earth Sciences and Geotechnical Engineering* 11: 203–247. https://doi.org/10.47260/jesge/1116.

Akhlaghi, Tohid, and Ali Nikkar. 2014. "Evaluation of the Pseudostatic Analyses of Earth Dams Using FE Simulation and Observed Earthquake-Induced Deformations: Case Studies of Upper San Fernando and Kitayama Dams.." *The Scientific World JOURNAL* 2014 (January):1–12. https://doi.org/10.1155/2014/585462.

Aljawhari, Karim., Gentile Roberto, and Galasso Carmine. 2022. "A Fragility-Oriented Approach for Seismic Retrofit Design." *Earthquake Spectra* 38 (3): 1813–43. https://doi.org/10.1177/87552930221078324.

Aquib, Tariq A., Jayalakshmi Sivasubramonian, and P. Martin Mai. 2022. "Analysis of Ground Motion Intensity Measures and Selection Techniques for Estimating Building Response." *Applied Sciences* 12 (23): 12089. https://doi.org/10.3390/app122312089

Arias, A. 1970. "A Measure of Earthquake Intensity." In *Seismic Design for Nuclear Power Plants*, edited by R. J. Hansen, 438–483. Cambridge, MA: MIT Press.

Armstrong, Richard J., Tadahiro Kishida, and Dong Soon Park. 2020. "Arias Intensity as a Predictor of Seismic Deformation in Earth Dams." *Soil Dynamics and Earthquake Engineering* 130:105986. https://doi.org/10.1016/j.soildyn.2019.105986.

Bahrampouri, Mahdi, Adrian Rodriguez-Marek, and Russell A Green. 2020. "Ground Motion Prediction Equations for Arias Intensity Using the Kik-net Database." *Earthquake Spectra* 37 (1): 428–448. https://doi.org/10.1177/8755293020938815.

Bakalis, Konstantinos, and Dimitrios Vamvatsikos. 2018. "Seismic Fragility Functions via Nonlinear Response History Analysis." *Journal of Structural Engineering* 144 (10): 10. https://doi.org/10.1061/(asce)st.1943-541x.0002141.

Baltay, Annemarie S., Thomas C. Hanks, and Norman A. Abrahamson. 2019. "Earthquake Stress Drop and Arias Intensity." *Journal of Geophysical Research: Solid Earth* 124 (4): 3838–3852. https://doi.org/10.1029/2018JB016753.

Beck, Marcus W., Andrea H. Claassen, and Peter J. Hundt. 2012. "Environmental and Livelihood Impacts of Dams: Common Lessons Across Development Gradients That Challenge Sustainability." *International Journal of River Basin Management* 10 (1): 73–92. https://doi.org/10.1080/15715124.2012.656133.

Benjamin, Jack R. 1988. "A Criterion for Determining Exceedance of the Operating Basis Earthquake." EPRI Report NP-5930.

Boore, David M., and Julian J. Bommer. 2004. "Processing of Strong-motion Accelerograms: Needs, Options and Consequences." *Soil Dynamics and Earthquake Engineering* 25 (2): 93–115. https://doi.org/10.1016/j.soildyn.2004.10.007.

Bradley, Brendon A. 2015. "Correlation of Arias Intensity with Amplitude, Duration, and Cumulative Intensity Measures." *Soil Dynamics and Earthquake Engineering* 78:89–98. https://doi.org/10.1016/j.soildyn.2015.07.009.

Bray, Jonathan D., and Thaleia Travasarou. 2007. "Simplified Procedure for Estimating Earthquake-Induced Deviatoric Slope Displacements." *Journal of Geotechnical and Geoenvironmental Engineering* 133 (4): 381–392. https://doi.org/10.1061/(ASCE)1090-0241(2007)133:4(381).

Broekhuizen, Henk, Catharina G. M. Groothuis-Oudshoorn, Janine A. van Til, J. Marjan Hummel, and Maarten J. IJzerman. 2015. "A Review and Classification of Approaches for Dealing with Uncertainty in Multi-Criteria Decision Analysis for Healthcare Decisions."

Pharmacoeconomics 33 (5): 445–455. https://doi.org/10.1007/s40273-014-0251-x.

Burman, A., Parsuram Nayak, P. Agrawal, and Damodar Maity. 2011. "Coupled Gravity Dam–foundation Analysis Using a Simplified Direct Method of Soil–structure Interaction." *Soil Dynamics and Earthquake Engineering* 34 (1): 62–68. https://doi.org/10.1016/j.soildyn.2011.10.008.

Busch, Andrew M. 2021. "Dams and the Age of Abundance: Hydraulic Boosterism, Regional Growth, and the Reemergence of Water Scarcity in Central Texas." *Journal of Urban History* 49 (2): 309–334. https://doi.org/10.1177/00961442211008865.

Chakraborty, Rubi, and Arindam Dey. 2024. "Probabilistic Assessment of Seismic Response of Toe-Excavated Partially Saturated Hillslopes." *Indian Geotechnical Journal* 54 (1): 196–209. https://doi.org/10.1007/s40098-023-00840-2.

Chen, Chen, Xiang Lu, Junru Li, Jiankang Chen, Zhengjun Zhou, and Liang Pei. 2021. "A Novel Settlement Forecasting Model for Rockfill Dams Based on Physical Causes." *Bulletin of Engineering Geology and the Environment* 80 (10): 7973–7988. https://doi.org/10.1007/s10064-021-02403-2.

Ciampoli, Marcello, and Paolo Giovenale. 2004. "Optimal Intensity Measures for the Characterization of the Ground Motion in Performance-Based Seismic Design." In *Springer eBooks*, 2932–37. https://doi.org/10.1007/978-0-85729-410-4_469.

Clarkson, Luke, David Williams, and Jaakko Seppälä. 2020. "Real-time Monitoring of Tailings Dams." *Georisk Assessment and Management of Risk for Engineered Systems and Geohazards* 15 (2): 113–127. https://doi.org/10.1080/17499518.2020.1740280.

Cornell, C. Allin, Fatemeh Jalayer, Ronald O. Hamburger, and Douglas A. Foutch. 2002. "Probabilistic Basis for 2000 SAC Federal Emergency Management Agency Steel Moment Frame Guidelines." *Journal of Structural Engineering* 128 (4): 526–533. https://doi.org/10.1061(ASCE)0733-9445(2002)128:4(526).

Cui, Chun-Yang. 2023. "Seismic Behavior and Reinforcement Mechanisms of Earth Dam and Liquefiable Foundation System by Shaking Table Tests and Numerical Simulation." *Soil Dynamics and Earthquake Engineering* 173 (June): 108083. https://doi.org/10.1016/j.soildyn.2023.108083

Danciu, L., and G.-A. Tselentis. 2007. "Engineering Ground-Motion Parameters Attenuation Relationships for Greece." *Bulletin of the Seismological Society of America* 97 (1B): 162–183. https://doi.org/10.1785/0120050087.

De La Paz-Bonilla, Ismael, and Aidcer L. Vidot-Vega. 2017. "Application of a Performance-displacement Based Method for the Seismic Assessment of Earth Dams." *International Journal of Geo-Engineering* 8 (1): 10. https://doi.org/10.1186/s40703-017-0048-9.

Dhiman, Sanchit, Gyanendra Kumar Chaturvedy, Umesh Kumar Pandey, and Sanjay Bhandari. 2024. "Seismic Behavior and Stability Analysis of an Embankment Dam on a Permeable Foundation." *Civil and Environmental Engineering Reports* 34 (2): 117–140. https://doi.org/10.59440/ceer/188637.

Federal Emergency Management Agency (FEMA). 2005. *Federal Guidelines for Dam Safety: Earthquake Analyses and Design of Dams (FEMA P-65)*. https://www.fema.gov/sites/default/files/2020-08/fema_dam-safety_earthquake-analysis_P-65.pdf.

Federal Emergency Management Agency (FEMA). 2020. *NEHRP Recommended Seismic Provisions for New Buildings and Other Structures. FEMA P-2082-1*. Washington, DC: U.S. Department of Homeland Security.

Fell, Robin, Patrick MacGregor, David Stapledon, and Graeme Bell. 2005. *Geotechnical Engineering of Dams*. Boca Raton, FL: CRC Press eBooks. https://doi.org/10.1201/noe0415364409.

Flenga, M. G., and M. J. Favvata. 2021. "Fragility Curves and Probabilistic Seismic Demand Models on the Seismic Assessment of RC Frames Subjected to Structural Pounding." *Applied Sciences* 11 (17): 8253. https://doi.org/10.3390/app11178253.

GEO-SLOPE International Ltd. 2024. *GeoStudio 2024*, Version 24.1.0.1406. Calgary, AB: Seequent. Computer software. https://www.seequent.com/products solutions/geo studio/.

Ghaemi, Arman, and Jean-Marie Konrad. 2023. "Empirical Relationships for Estimating the Crest Settlement of Earth-core Rockfill Dams Subjected to Earthquakes.." *Canadian Geotechnical Journal* 60 (2): 166–81. https://doi.org/10.1139/cgj-2021-0159.

Ghahreman-Nejad, Bahareh, and Maryam E. Kan. 2017. "Seismic Deformation Analysis of Embankment Dams: A Comparison between Simplified and Non-linear Numerical Methods."

Giovenale, Paolo, C. Allin Cornell, and Luis Esteva. 2004. "Comparing the Adequacy of Alternative Ground Motion Intensity Measures for the Estimation of Structural Responses." *Earthquake Engineering & Structural Dynamics* 33 (8): 951–979. https://doi.org/10.1002/eqe.386.

Giusto, M., et al. 2025. "Performance-Based Seismic Design Framework for Earth Dams." *Earthquake Spectra* 41 (1): 55–78. https://doi.org/10.1193/090123EQS389M.

Gordan, Behrouz, Mohammad Asif Raja, Danial Jahed Armaghani, and Azlan Adnan. 2021. "Review on Dynamic Behaviour of Earth Dam and Embankment During an Earthquake." *Geotechnical and Geological Engineering* 40 (1): 3–33. https://doi.org/10.1007/s10706-021-01919-4.

Guo, Xiangfeng, Daniel Dias, and Qiujing Pan. 2019. "Probabilistic Stability Analysis of an Embankment Dam Considering Soil Spatial Variability." *Computers and Geotechnics* 113 (May): 103093. https://doi.org/10.1016/j.compgeo.2019.103093.

Han, Heuisoo, Mincheol Park, Sangki Park, Juhyong Kim, and Yong Baek. 2019. "Experimental Verification of Methods for Converting Acceleration Data in High-Rise Buildings into Displacement Data by Shaking Table Test." *Applied Sciences* 9 (8): 1653. https://doi.org/10.3390/app9081653

Hariri-Ardebili, Mohammad Amin, Siyu Chen, and Golsa Mahdavi. 2022. "Machine Learning-aided PSDM for Dams With Stochastic Ground Motions." *Advanced Engineering Informatics* 52: 101615 https://doi.org/10.1016/j.aei.2022.101615.

He, Jingwen, and Ellen M. Rathje. 2024. "Seismic Capacity Models for Earth Dams and Their Use in Developing

Fragility Curves." *Earthquake Spectra* 40 (3): 1986–2007. https://doi.org/10.1177/87552930241243067.

Heresi, Pablo, and Eduardo Miranda. 2023. "RPBEE: Performance-based Earthquake Engineering on a Regional Scale." *Earthquake Spectra* 39 (3): 1328–1351. https://doi.org/10.1177/87552930231179491.

Hongqiang, Chunxia Fu, Yangjuan Bao, Ling Liu, Sheng Shi, Fengjin Zhu, Min Xiong, Baoping Zou, and Wengen Wang. 2025. "Seismic Fragility Assessment of Slopes with Scalar-valued and Vector-valued Earthquake Intensity Measures." *Acta Geotechnica* 20 (8): 3871–86. https://doi.org/10.1007/s11440-025-02606-x.

Housner, G. W. 1952. "Spectrum Intensities of Strong-Motion Earthquakes." In *Proceedings of the Symposium on Earthquakes and Blast Effects on Structures, Vol. 2*, 21–36.

Housner, G. W., and Paul C. Jennings. 1964. "Generation of Artificial Earthquakes." *Journal of the Engineering Mechanics Division* 90 (1): 113–150. https://doi.org/10.1061/JMCEA3.0000448.

Hu, Hongqiang, Gang Gan, Linyong Cui, Tangdai Xia, Lin Wang, and Xu Han. 2023. "Nonparametric Representation for Seismic Fragility Assessment of Earth Dams With Spatially Variable Soil Properties." *International Journal of Geomechanics* 23 (8): 04023108. https://doi.org/10.1061/ijgnai.gmeng-7266.

Hu, Hongqiang, Yu Huang, Min Xiong, and Liuyuan Zhao. 2021. "Investigation of Seismic Behavior of Slope Reinforced by Anchored Pile Structures Using Shaking Table Tests." *Soil Dynamics and Earthquake Engineering* 150 (July): 106900. https://doi.org/10.1016/j.soildyn.2021.106900.

Huang, Yin-Nan, Andrew S. Whittaker, Nicolas Luco, and Ronald O. Hamburger. 2009. "Scaling Earthquake Ground Motions for Performance-Based Assessment of Buildings." *Journal of Structural Engineering* 137 (3): 311–321. https://doi.org/10.1061/(ASCE)ST.1943-541X.0000155.

Huang, Zhong-Kai, Kyriazis Pitilakis, Sotirios Argyroudis, Grigorios Tsinidis, and Dong-Mei Zhang. 2021. "Selection of Optimal Intensity Measures for Fragility Assessment of Circular Tunnels in Soft Soil Deposits." *Soil Dynamics and Earthquake Engineering* 145 (March): 106724. https://doi.org/10.1016/j.soildyn.2021.106724.

Hurtado-López, Grissel, and Juan Manuel Mayoral-Villa. 2019. "Fragility Curves for Hardfill Dams Under Seismic Loading." *Tecnología Y Ciencias Del Agua* 11 (1): 132–168. https://doi.org/10.24850/j-tyca-2020-01-04.

Hwang, Ching-Lai, and Kwangsun Yoon. 1981. *Multiple Attribute Decision Making. Lecture Notes in Economics and Mathematical Systems*.

International Commission on Large Dams (ICOLD). 2010. *Selecting Seismic Parameters for Large Dams (Bulletin 148)*. https://www.icoldchile.cl/boletines/148.pdf.

Ishibashi, Isao, and Xinjian Zhang. 1993. "Unified Dynamic Shear Moduli and Damping Ratios of Sand and Clay." *Soils and Foundations* 33 (1): 182–191. https://doi.org/10.3208/sandf1972.33.182.

Jalayer, Fatemeh, and C. Allin Cornell. 2009. "Alternative Nonlinear Demand Estimation Methods for Probability-Based Seismic Assessments." *Earthquake Engineering & Structural Dynamics* 38 (8): 951–972. https://doi.org/10.1002/eqe.876.

Jiang, Shu, Rong-Jun Zhang, Jun-Jie Zheng, and Zi-Qian Li. 2025. "An Analysis Framework Integrating Stochastic Stratigraphic Modelling and Probabilistic Analysis in Tunnel Engineering." *Georisk Assessment and Management of Risk for Engineered Systems and Geohazards*: 1–19. https://doi.org/10.1080/17499518.2025.2561064.

Kennedy, R. P., C. A. Cornell, R. D. Campbell, S. Kaplan, and H. F. Perla. 1980. "Probabilistic Seismic Safety Study of an Existing Nuclear Power Plant." *Nuclear Engineering and Design* 59 (2): 315–338. https://doi.org/10.1016/0029-5493(80)90203-4.

Khalid, Muhammad Irslan, Duhee Park, Jianbo Fei, Van-Quang Nguyen, Duy-Duan Nguyen, and Xiangsheng Chen. 2023. "Selection of Efficient Earthquake Intensity Measures for Evaluating Seismic Fragility of Concrete Face Rockfill Dam." *Computers and Geotechnics* 163 (August): 105721. https://doi.org/10.1016/j.compgeo.2023.105721.

Khalilzad, Mahdi, Mohammed A. Gabr, and Mary Ellen Hynes. 2015. "Assessment of Remedial Measures to Reduce Exceedance Probability of Performance Limit States in Embankment Dams." *Computers and Geotechnics* 67:213–222. https://doi.org/10.1016/j.compgeo.2015.02.010

Khanmohammadi, Mohammad, Majid Eshraghi, Sina Sayadi, and Milad Ghafarian Mashhadinezhad. 2023. "Post-earthquake Seismic Assessment of Residential Buildings Following Sarpol-e Zahab (Iran) Earthquake (Mw7.3) Part 1: Damage Types and Damage States." *Soil Dynamics and Earthquake Engineering* 173 (July): 108121. https://doi.org/10.1016/j.soildyn.2023.108121.

Khosravikia, Farid, and Patricia Clayton. 2019. "Updated Evaluation Metrics for Optimal Intensity Measure Selection in Probabilistic Seismic Demand Models." *Engineering Structures* 202 (November): 109899. https://doi.org/10.1016/j.engstruct.2019.109899

Kramer, Steven L., and Jonathan P. Stewart. 2024. *Geotechnical Earthquake Engineering*. https://doi.org/10.1201/9781003512011.

Kwak, D. Y., J. P. Stewart, S. J. Brandenberg, and A. Mikami. 2016. "Characterization of Seismic Levee Fragility Using Field Performance Data." *Earthquake Spectra* 32 (1): 193–215. https://doi.org/10.1193/030414EQS035M

Lee, Kevin Zeh-Zon, Navead Jensen, David R. Gillette, and Derek T. Wittwer. 2019. "Seismic Deformation Analysis of Embankment Dams Using Simplified Total-Stress Approach." *Journal of Geotechnical and Geoenvironmental Engineering* 145 (10): 04019076. https://doi.org/10.1061/(asce)gt.1943-5606.0002135.

Limpert, Erhard, Walter A. Stahel, and Martin Abbt. 2001. "Log-Normal Distributions across the Sciences: Keys and Clues." *BioScience* 51 (5): 341–352. https://doi.org/10.1641/0006-3568(2001)051[0341:LNDATS]2.0.CO;2

Liu, Z. 2024. *Seismic Risk Assessment of Spatially Distributed Levee System in the Sacramento–San Joaquin Delta*. PhD diss., University of California, Los Angeles.

Liu, Zhongqiang, Farrokh Nadim, Alexander Garcia-Aristizabal, Arnaud Mignan, Kevin Fleming, and Byron Quan Luna. 2015. "A Three-level Framework for Multi-risk Assessment." *Georisk Assessment and Management of Risk for Engineered Systems and Geohazards* 9 (2): 59–74. https://doi.org/10.1080/17499518.2015.1041989.

Lozano, Jorge-Mario, and Iris Tien. 2023. "Data Collection Tools for Post-disaster Damage Assessment of Building and Lifeline Infrastructure Systems." *International Journal of Disaster Risk Reduction* 94 (June): 103819. https://doi.org/10.1016/j.ijdrr.2023.103819

Luco, Nicolas, and C. Allin Cornell. 2007. "Structure-Specific Scalar Intensity Measures for Near-Source and Ordinary Earthquake Ground Motions." *Earthquake Spectra* 23 (2): 357–392. https://doi.org/10.1193/1.2723158.

Lulić, Luka, Karlo Ožić, Tomislav Kišiček, Ivan Hafner, and Mislav Stepinac. 2021. "Post-Earthquake Damage Assessment – Case Study of the Educational Building After the Zagreb Earthquake." *Sustainability* 13 (11): 6353. https://doi.org/10.3390/su13116353.

Lysmer, John, and Roger L. Kuhlemeyer. 1969. "Finite Dynamic Model for Infinite Media." *Journal of the Engineering Mechanics Division* 95 (4): 859–877. https://doi.org/10.1061/JMCEA3.0001144

Macedo, J., et al. 2015. "Simulation-Based Probabilistic Seismic Demand Models for Earth Dams." *Soil Dynamics and Earthquake Engineering* 77:136–148.

Mackie, Kevin, and Božidar Stojadinović. 2001. "Probabilistic Seismic Demand Model for California Highway Bridges." *Journal of Bridge Engineering* 6 (6): 468–481. https://doi.org/10.1061/(ASCE)1084-0702(2001)6:6(468)

Mazurek, Jiří, and Dominik Strzałka. 2022. "On the Monte Carlo Weights in Multiple Criteria Decision Analysis." *PLoS One* 17 (10): e0268950. https://doi.org/10.1371/journal.pone.0268950

Moehle, J., and G. Deierlein. 2004. "A Framework Methodology for Performance-Based Earthquake Engineering." In *Proceedings of the 13th World Conference on Earthquake Engineering, Vancouver, Canada*.

Nardo, A., G. Biondi, and E. Cascone. 2024. "Evaluation of Seismic-induced Crest Settlement of Earth Dams." In *CRC Press eBooks*, 1846–51.

Newmark, N. M. 1965. "Effects of Earthquakes on Dams and Embankments." *Geotechnique* 15 (2): 139–160. https://doi.org/10.1680/geot.1965.15.2.139.

Nuttli, Otto W. 1979. *The Relation of Sustained Maximum Ground Acceleration and Velocity to Earthquake Intensity and Magnitude*. Vicksburg, MS: US Army Engineer Waterways Experiment Station. ".

Padgett, Jamie E., Bryant G. Nielson, and Reginald DesRoches. 2007. "Selection of Optimal Intensity Measures in Probabilistic Seismic Demand Models of Highway Bridge Portfolios." *Earthquake Engineering & Structural Dynamics* 37 (5): 711–725. https://doi.org/10.1002/eqe.782

Papadimitriou, A. G., G. D. Bouckovalas, and K. I. Andrianopoulos. 2014. "Methodology for Estimating Seismic Coefficients for Performance-Based Design of Earth Dams and Tall Embankments." *Soil Dynamics and Earthquake Engineering* 56:57–73. https://doi.org/10.1016/j.soildyn.2013.10.006

Pells, S., and R. Fell. 2003. "Damage and Cracking of Embankment Dams by Earthquake and the Implications for Internal Erosion and Piping." Paper Q.83-R.17, *Proceedings of the 21st Congress, International Commission on Large Dams (ICOLD), Montreal, June 2003*.

Peng, Ming, Yaoying Liang, Haofeng Xing, Ge Yang, Yan Zhu, Limin Zhang, Bingxin Li, Shuo Cai, and Jingchao Bi. 2025. "Stochastic Seepage Stability Analysis of the Pubugou Clay Core Rockfill Dam With Potentially High Permeability Zone by Integrating Multi-source Monitoring Information." *Georisk Assessment and Management of Risk for Engineered Systems and Geohazards* 19 (2): 427–447. https://doi.org/10.1080/17499518.2024.2445929.

Pinzón, Luis A., Diego A. Hidalgo-Leiva, Rodrigo E. Alva, Miguel A. Mánica, and Luis G. Pujades. 2023. "Correlation Between Seismic Intensity Measures and Engineering Demand Parameters of Reinforced Concrete Frame Buildings Through Nonlinear Time History Analysis." *Structures* 57 (September): 105276. https://doi.org/10.1016/j.istruc.2023.105276

Priestley, M. J. N., and M. J. Kowalsky. 2000. "Direct Displacement-based Seismic Design of Concrete Buildings." *Bulletin of the New Zealand Society for Earthquake Engineering* 33 (4): 421–444. https://doi.org/10.5459/bnzsee.33.4.421-444.

Qi, Hui, Rui Sun, Jianfeng Chen, Ming Peng, Ning Bao, and Xinzhuang Cui. 2024. "Stochastic Seismic Performance of Slopes Reinforced by a Combination of Piles and Anchor Cables Using the Probability Density Evolution Method." *Georisk Assessment and Management of Risk for Engineered Systems and Geohazards* 19 (3): 555–572. https://doi.org/10.1080/17499518.2024.2443536.

Rathje, Ellen M., Norman A. Abrahamson, and Jonathan D. Bray. 1998. "Simplified Frequency Content Estimates of Earthquake Ground Motions." *Journal of Geotechnical and Geoenvironmental Engineering* 124 (2): 150–159. https://doi.org/10.1061/(ASCE)1090-0241(1998)124:2(150)

Rathje, Ellen M., and George Antonakos. 2011. "A Unified Model for Predicting Earthquake-Induced Sliding Displacements of Rigid and Flexible Slopes." *Engineering Geology* 122 (1–2): 51–60. https://doi.org/10.1016/j.enggeo.2010.12.004.

Rathje, Ellen M., and Jingwen He. 2022. "A Seismic Fragility Framework for Earth Dams." *Lifelines* 2022:405–415. https://doi.org/10.1061/9780784484432.036.

Reed, John W., and Robert P. Kassawara. 1990. "A Criterion for Determining Exceedance of the Operating Basis Earthquake." *Nuclear Engineering and Design* 123 (2–3): 387–396. https://doi.org/10.1016/0029-5493(90)90259-z.

Regina, Gianluca, Paolo Zimmaro, Katerina Ziotopoulou, and Roberto Cairo. 2023. "Evaluation of the Optimal Ground Motion Intensity Measure in the Prediction of the Seismic Vulnerability of Earth Dams." *Earthquake Spectra* 39 (4): 2352–2378. https://doi.org/10.1177/87552930231170894

Saeidi, Ali, Esmaeil Eslami, Marco Quirion, and Mahdiyeh Seifaddini. 2019. "Assessment of Rock Mass Erosion in Unlined Spillways Using Developed Vulnerability and Fragility Functions." *Georisk Assessment and Management of Risk for Engineered Systems and Geohazards* 14 (4): 280–292. https://doi.org/10.1080/17499518.2019.1660796.

Salazar, Fernando, and Mohammad Amin Hariri-Ardebili. 2022. "Coupling Machine Learning and Stochastic Finite Element to Evaluate Heterogeneous Concrete Infrastructure." *Engineering Structures* 260: 114190 https://doi.org/10.1016/j.engstruct.2022.114190.

Saltelli, Andrea, Marco Ratto, Terry Andres, Francesca Campolongo, Jessica Cariboni, Debora Gatelli, Michaela Saisana, and Stefano Tarantola. 2008. *Global Sensitivity Analysis: The Primer*. Chichester: John Wiley & Sons. https://doi.org/10.1002/9780470725184

Schleiss, Anton J. 2018. "Sustainable and Safe Development of Dams and Reservoirs as Vital Water Infrastructures in This Century – The Important Role of ICOLD." In *Proceedings of the International Dam Safety Conference*, 3–17.

Seed, H. B. 1965. "Considerations in the Earthquake-Resistant Design of Earth and Rockfill Dams." *Geotechnique* 15 (2): 139–160. https://doi.org/10.1680/geot.1965.15.2.139.

SeismoSoft. 2024. SeismoSignal 2024, Version 2024. Pavia, Italy: SeismoSoft. Computer software. https://www.seismosoft.com.

Swaisgood, J. R. 2003. "Embankment Dam Deformations Caused by Earthquakes." In *Pacific conference on earthquake engineering*, vol. 14.

Tan, Chong, Yushi Lu, and Xiaotao Zhang. 2016. "Life Extension and Repair Decision-making of Ageing Offshore Platforms Based on DHGF Method." *Ocean Engineering* 117 (March): 238–245. https://doi.org/10.1016/j.oceaneng.2016.03.048.

Tang, Liang, Yi Zhang, Xianzhang Ling, and Shuang Tian. 2022. "Fuzzy Optimization for Ground Motion Intensity Measures to Characterize the Response of the Pile-supported Wharf in Liquefiable Soils." *Ocean Engineering* 265 (September): 112645. https://doi.org/10.1016/j.oceaneng.2022.112645

Tao, Dongwang, Haifeng Zhang, Shanyou Li, Jianqi Lu, Zhinan Xie, and Qiang Ma. 2024. "Predictive Model for Peak Ground Velocity Using Long Short-term Memory Networks." *Journal of Seismology* 29 (1): 221–240. https://doi.org/10.1007/s10950-024-10268-7.

Tartaglia, Roberto, Mario D'Aniello, and Raffaele Landolfo. 2022. "Seismic Performance of Eurocode-Compliant Ductile Steel MRFs." *Earthquake Engineering & Structural Dynamics* 51 (11): 2527–2552. https://doi.org/10.1002/eqe.3672

U.S. Army Corps of Engineers , (USACE). 2024. *ER 1110-2-1806: Earthquake Analysis, Evaluation, and Design for Civil Works Projects*. Washington, DC: U.S. Army Corps of Engineers. Effective 29 May 2024.

U.S. Army Corps of Engineers (USACE). 1995. *Instrumentation of Embankment Dams and Levees*.

U.S. Army Corps of Engineers (USACE). 2007. *Earthquake Design and Evaluation of Concrete Hydraulic Structures. EM 1110-2-6053*. Washington, DC: U.S. Army Corps of Engineers.

U.S. Society on Dams (USSD). 2022. *Analysis of Seismic Deformations of Embankment Dams State-of-Practice Guidance*.

Vahedifard, F., and C. Meehan. 2011. "Multi-Parameter Regression Equations for Newmark Displacements of Earth Dams." *Engineering Geology* 122 (1–2): 70–80.

Vargas-Alzate, Yeudy F., Jorge E. Hurtado, and Luis G. Pujades. 2021. "New Insights into the Relationship Between Seismic Intensity Measures and Nonlinear Structural Response." *Bulletin of Earthquake Engineering* 20 (5): 2329–2365. https://doi.org/10.1007/s10518-021-01283-x

Wang, Shaowei, Chongshi Gu, Yi Liu, Hao Gu, Bo Xu, and Bangbin Wu. 2024. "Displacement observation data-based structural health monitoring of concrete dams: A state-of-art review." *Structures* 68: 107072. https://doi.org/10.1016/j.istruc.2024.107072.

Wang, Xiaowei, Abdollah Shafieezadeh, and Aijun Ye. 2017. "Optimal Intensity Measures for Probabilistic Seismic Demand Modeling of Extended Pile-shaft-supported Bridges in Liquefied and Laterally Spreading Ground." *Bulletin of Earthquake Engineering* 16 (1): 229–257. https://doi.org/10.1007/s10518-017-0199-2.

Więckowski, Jakub, and Wojciech Sałabun. 2023. "Sensitivity Analysis Approaches in Multi-Criteria Decision Analysis: A Systematic Review." *Applied Soft Computing* 148:110915. https://doi.org/10.1016/j.asoc.2023.110915.

Xin, Yuan, Bu Henan, Niu Jianmin, Yu Wenjuan, Zhou Honggen, Ji Xingyu, and Ye Pengfei. 2021. "Coating Matching Recommendation Based on Improved Fuzzy Comprehensive Evaluation and Collaborative Filtering Algorithm." *Scientific Reports* 11 (1). 14035. https://doi.org/10.1038/s41598-021-93628-4.

Xu, Bin, and Rui Pang. 2024. "Probability Analysis Method of Seismic Response for Earth-Rockfill Dams." *Hydroscience and Engineering* 19–59. https://doi.org/10.1007/978-981-97-7198-1_2.

Xue, Xinhua, and Xingguo Yang. 2014. "Seismic liquefaction potential assessed by fuzzy comprehensive evaluation method." *Natural Hazards* 71 (3): 2101–2112. https://doi.org/10.1007/s11069-013-0997-z.

Yakut, Ahmet, and Hazım Yılmaz. 2008. "Correlation of Deformation Demands with Ground Motion Intensity." *Journal of Structural Engineering* 134 (12): 1818–1828. https://doi.org/10.1061/(ASCE)0733-9445(2008)134:12(1818).

Zentner, I., N. Humbert, S. Ravet, and E. Viallet. 2011. "Numerical Methods for Seismic Fragility Analysis of Structures and Components in Nuclear Industry - Application to a Reactor Coolant System." *Georisk Assessment and Management of Risk for Engineered Systems and Geohazards* 5 (2): 99–109. https://doi.org/10.1080/17499511003630512

Zerbe, Richard O., and Anthony Falit-Baiamonte. 2001. "The Use of Benefit-Cost Analysis for Evaluation of Performance-Based Earthquake Engineering Decisions." *UW Tacoma Digital Commons*. https://digitalcommons.tacoma.uw.edu/urban_pub/11/.

Zhang, L. M., Y. Xu, and J. S. Jia. 2009. "Analysis of Earth Dam Failures: A Database Approach." *Georisk Assessment and Management of Risk for Engineered Systems and Geohazards* 3 (3): 184–189. https://doi.org/10.1080/17499510902831759

Zhang, Xiaolong, Shuai Huang, Binhai Gao, and Haitao Qian. 2025. "Intelligent Risk Assessment of Co-seismic Landslide Susceptibility Using Multi-directional Seismic Ground Motion Parameters." *Georisk Assessment and Management of Risk for Engineered Systems and Geohazards* 1–24. https://doi.org/10.1080/17499518.2025.2567480.

Zhang, Xiaoyu, Yingyi Pan, Lei Su, Entong Ou, Hai Liu, Chao Liu, and Jie Cui. 2024. "Seismic Fragility Assessment of Shield Tunnels in Liquefiable Soil-rock Strata Using Fuzzy Method for IM Optimization." *Tunnelling and Underground Space Technology* 152 (July): 105957. https://doi.org/10.1016/j.tust.2024.105957

Zheng, Shiying, Shin-Ichi Nishimura, Takayuki Shuku, Toshifumi Shibata, and Tsubasa Tateishi. 2023. "Risk

Evaluation for Earth-fill Dams Due to Heavy Rains by Response Surface Method." *Georisk Assessment and Management of Risk for Engineered Systems and Geohazards* 17 (3): 572–585. https://doi.org/10.1080/17499518.2023.2164901

Appendix A

Intensity measure (IM) description and properties

Ground motion parameters encompass at least one of the three fundamental characteristics of an earthquake: amplitude, frequency content, and duration (Kramer and Stewart 2024). The 14 different Intensity Measures (IMs) analyzed in this study are outlined below. The parameters Peak Ground Acceleration (PGA), Peak Ground Velocity (PGV), and Peak Ground Displacement (PGD) reflect the maximum amplitudes of acceleration, velocity, and displacement recorded (Kramer and Stewart 2024):

(1) Peak ground acceleration (PGA) is the maximum ground acceleration recorded during an earthquake and is given by:

$$PGA = \max|a(t)|$$

(2) Peak ground velocity (PGV) is the maximum ground velocity (first integration of acceleration) and is given by:

$$PGV = \max|v(t)|$$

(3) Peak ground displacement (PGD) is the maximum ground displacement (double integration of acceleration) and is given by:

$$PGD = \max|d(t)|$$

(4) Sustained Maximum acceleration (SMA):

Nuttli (1979) introduced this parameter, representing the sustained maximum acceleration recorded over three cycles. It is defined as the third highest absolute value of acceleration within the time history, where a value must exceed those recorded 20 steps before and 20 steps after to be considered a "maximum."

$$SMA = \textit{the 3rd highest } |a(t)|$$

(5) Sustained Maximum Velocity (SMV):

Nuttli (1979) introduced this parameter, which represents the sustained maximum velocity achieved during three cycles. It is defined as the third-highest absolute value of velocity in the time history. It is important to note that for an absolute value to be classified as a "maximum", it must surpass the values recorded 20 steps before and 20 steps after it.

$$SMV = \textit{the 3rd highest } |v(t)|$$

(6) The ratio of PGV and PGA is given by:

$$\frac{PGV}{PGA} = \frac{\max|v(t)|}{\max|a(t)|}$$

(7) Mean period (MP) is defined as:

$$MP = \frac{\sum_i C_i^2 \left(\frac{1}{f_i}\right)}{\sum_i C_i^2} \quad for \;\; 0.25\ Hz \le f_i \le 20Hz$$

where C_i = Fourier amplitudes of the entire accelerogram; f_i = discrete Fourier transform frequencies between 0.25 and 20 Hz (Rathje, Abrahamson, and Bray 1998).

(8) The predominant period (PP) is defined as the period of vibration corresponding to the maximum value of the smoothed Fourier amplitude spectrum calculated at 5% damping (Kramer and Stewart 2024).

(9) The root mean square acceleration (ARMS) is the effective (RMS) acceleration over the significant duration and is defined as:

$$ARMS = \sqrt{\frac{1}{t_{total}} \int_0^{t_{total}} a(t)^2 dt}$$

(10) The root mean square velocity (VRMS) is the RMS of velocity over the record and is defined as:

$$VRMS = \sqrt{\frac{1}{t_{total}} \int_0^{t_{total}} v(t)^2 dt}$$

(11) The root mean square displacement (DRMS) is the RMS of displacement over the record and is defined as:

$$DRMS = \sqrt{\frac{1}{t_{total}} \int_0^{t_{total}} d(t)^2 dt}$$

(12) The Arias Intensity (AI) is computed as:

$$AI = \frac{\pi}{2g} \int_0^{t_{total}} [a(t)]^2 dt$$

(13) The Cumulative Absolute Velocity CAV is computed as:

$$CAV = \int_0^{t_{total}} [a(t)] dt$$

(14) Effective Design Acceleration (EDA):

This parameter corresponds to the peak acceleration value identified after low-pass filtering of the input time history with a cut-off frequency of 9 Hz (Benjamin 1988).